From high $p_\perp$ theory and data to inferring the anisotropy of quark-gluon plasma

Stefan Stojku, Institute of Physics Belgrade

in collaboration with: Magdalena Djordjevic, Marko Djordjevic and Pasi Huovinen

МИНИСТАРСТВО ПРОСВЕТЕ,
НАУКЕ И ТЕХНОЛОШКОГ РАЗВОЈА

Introduction

- Energy loss of high energy particles traversing QCD medium is an excellent probe of QGP properties.

- Energy loss of high energy particles traversing QCD medium is an excellent probe of QGP properties.
- High energy particles:
  - Are produced only during the initial stage of QCD matter

- Energy loss of high energy particles traversing QCD medium is an excellent probe of QGP properties.
- High energy particles:
  - Are produced only during the initial stage of QCD matter
  - Significantly interact with the QCD medium

Introduction

- Energy loss of high energy particles traversing QCD medium is an excellent probe of QGP properties.
- High energy particles:
  - Are produced only during the initial stage of QCD matter
  - Significantly interact with the QCD medium
  - Perturbative calculations are possible

Introduction

- Energy loss of high energy particles traversing QCD medium is an excellent probe of QGP properties.
- High energy particles:
  - Are produced only during the initial stage of QCD matter
  - Significantly interact with the QCD medium
  - Perturbative calculations are possible
- Theoretical predictions can be:
  - compared with a wide range of experimental data

- Energy loss of high energy particles traversing QCD medium is an excellent probe of QGP properties.
- High energy particles:
  - Are produced only during the initial stage of QCD matter
  - Significantly interact with the QCD medium
  - Perturbative calculations are possible
- Theoretical predictions can be:
  - compared with a wide range of experimental data
  - used together with low-$p_\perp$ theory and experiments to study the properties of created QCD medium

- Energy loss of high energy particles traversing QCD medium is an excellent probe of QGP properties.
- High energy particles:
  - Are produced only during the initial stage of QCD matter
  - Significantly interact with the QCD medium
  - Perturbative calculations are possible
- Theoretical predictions can be:
  - compared with a wide range of experimental data
  - used together with low-$p_\perp$ theory and experiments to study the properties of created QCD medium
- Today - an example of how high-$p_\perp$ theory and data can be used to infer a geometric property of bulk QCD medium.

DREENA FRAMEWORK

- Our state-of-the-art dynamical energy loss formalism is embedded in DREENA framework.

DREENA FRAMEWORK

- Our state-of-the-art dynamical energy loss formalism is embedded in DREENA framework.
- **D**ynamic **R**adiative and **E**lastic **EN**ergy loss **A**pproach

- Our state-of-the-art dynamical energy loss formalism is embedded in DREENA framework.
- **D**ynamic **R**adiative and **E**lastic **EN**ergy loss **A**pproach
- A versatile and fully optimized procedure, capable of generating high $p_\perp$ predictions.

- Our state-of-the-art dynamical energy loss formalism is embedded in DREENA framework.
- **D**ynamic **R**adiative and **E**lastic **EN**ergy loss **A**pproach
- A versatile and fully optimized procedure, capable of generating high $p_\perp$ predictions.
- Includes:
  - Parton production

DREENA FRAMEWORK

- Our state-of-the-art dynamical energy loss formalism is embedded in DREENA framework.
- **D**ynamic **R**adiative and **E**lastic **EN**ergy loss **A**pproach
- A versatile and fully optimized procedure, capable of generating high $p_\perp$ predictions.
- Includes:
    - Parton production
    - Multi-gluon fluctuations

DREENA FRAMEWORK

- Our state-of-the-art dynamical energy loss formalism is embedded in DREENA framework.
- **D**ynamic **R**adiative and **E**lastic **EN**ergy loss **A**pproach
- A versatile and fully optimized procedure, capable of generating high $p_\perp$ predictions.
- Includes:
  - Parton production
  - Multi-gluon fluctuations
  - Path-length fluctuations

DREENA FRAMEWORK

- Our state-of-the-art dynamical energy loss formalism is embedded in DREENA framework.
- **D**ynamic **R**adiative and **E**lastic **EN**ergy loss **A**pproach
- A versatile and fully optimized procedure, capable of generating high $p_\perp$ predictions.
- Includes:
  - Parton production
  - Multi-gluon fluctuations
  - Path-length fluctuations
  - Fragmentation functions

DREENA FRAMEWORK

- Our state-of-the-art dynamical energy loss formalism is embedded in DREENA framework.
- **D**ynamic **R**adiative and **E**lastic **EN**ergy loss **A**pproach
- A versatile and fully optimized procedure, capable of generating high $p_\perp$ predictions.
- Includes:
  - Parton production
  - Multi-gluon fluctuations
  - Path-length fluctuations
  - Fragmentation functions
- Goal: include complex medium temperature evolution, while keeping all the elements of the state-of-the-art dynamical energy loss formalism!

- DREENA-**B**: 1+1D **B**jorken evolution

- DREENA-**B**: 1+1D **B**jorken evolution
- Medium evolution is implemented through an analytical expression - temperature is only a function of time.

D. Zigic, I. Salom, J. Auvinen, M. Djordjevic and M. Djordjevic, Phys. Lett. B791, 236 (2019).

- DREENA-B results: charged hadrons, $Pb + Pb$, $\sqrt{s_{NN}} = 5.02 TeV$

D. Zigic, I. Salom, J. Auvinen, M. Djordjevic and M. Djordjevic, Phys. Lett. B **791**, 236 (2019).

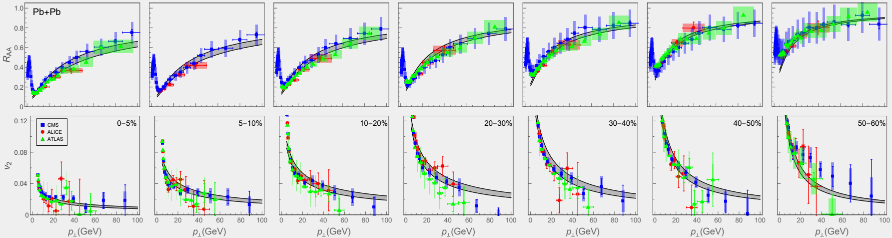

- DREENA-B results: charged hadrons, $Pb + Pb$, $\sqrt{s_{NN}} = 5.02 TeV$

D. Zigic, I. Salom, J. Auvinen, M. Djordjevic and M. Djordjevic, Phys. Lett. B **791**, 236 (2019).

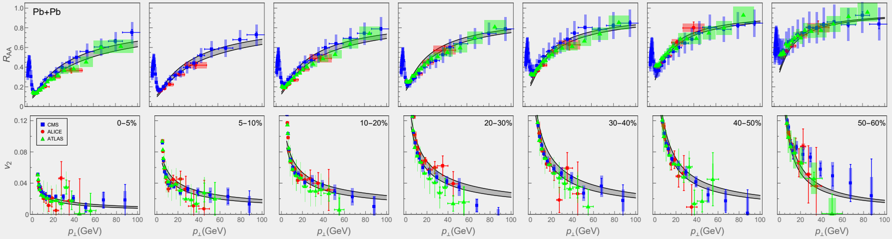

Very good joint agreement with both R_{AA} and v_2 data.

- DREENA-**A**: **A**daptive

- DREENA-**A**: **A**daptive
- Main goal of our research.

- DREENA-**A**: **A**daptive
- Main goal of our research.
- Tool for exploiting high-$p_\perp$ data for QGP tomography by using an advanced medium model.

- DREENA-**A**: **A**daptive
- Main goal of our research.
- Tool for exploiting high-$p_\perp$ data for QGP tomography by using an advanced medium model.
- DREENA-A introduces full medium evolution - but not at the expense of simplified energy loss.

DREENA FRAMEWORK

- DREENA-**A**: **A**daptive
- Main goal of our research.
- Tool for exploiting high-$p_\perp$ data for QGP tomography by using an advanced medium model.
- DREENA-A introduces full medium evolution - but not at the expense of simplified energy loss.
- In this talk: preliminary DREENA-A results for 3+1D hydro temperature profile

  E. Molnar, H. Holopainen, P. Huovinen and H. Niemi, Phys. Rev. C **90**, no. 4, 044904 (2014).

- DREENA-A results: charged hadrons, $Pb + Pb$, $\sqrt{s_{NN}} = 5.02TeV$

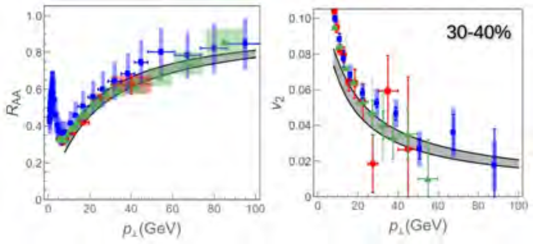

- DREENA-A results: charged hadrons, $Pb + Pb$, $\sqrt{s_{NN}} = 5.02 TeV$

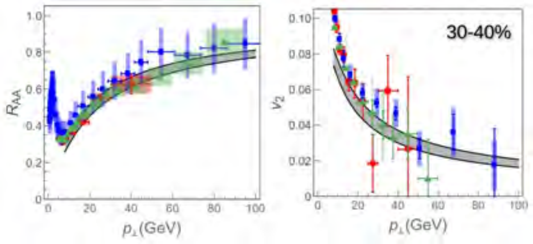

Very good joint agreement with R_{AA} and v_2 data!
(No fitting parameters.)

- DREENA-A results: charged hadrons, $Pb + Pb$, $\sqrt{s_{NN}} = 5.02 TeV$

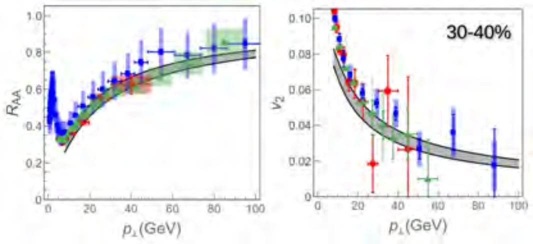

Very good joint agreement with R_{AA} and v_2 data!
(No fitting parameters.)

For high-$p_\perp$ data, proper description of parton-medium interactions is more important than medium evolution!

- Next goal: use high-$p_\perp$ data to infer bulk properties of QGP.

- **Next goal:** use high-$p_\perp$ data to infer bulk properties of QGP.

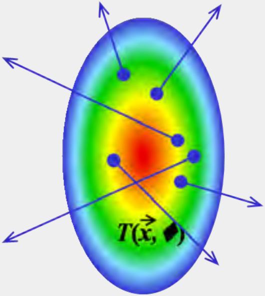

- High energy particles lose energy when they traverse QGP.

- Next goal: use high-$p_\perp$ data to infer bulk properties of QGP.

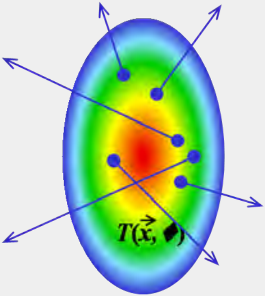

- High energy particles lose energy when they traverse QGP.
- This energy loss is sensitive to QGP properties.

- Next goal: use high-$p_\perp$ data to infer bulk properties of QGP.

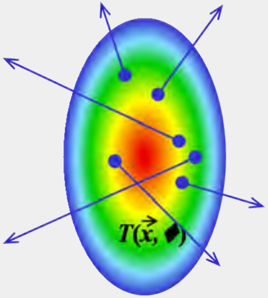

- High energy particles lose energy when they traverse QGP.
- This energy loss is sensitive to QGP properties.
- We can realistically predict this energy loss.

QGP TOMOGRAPHY

- Next goal: use high-$p_\perp$ data to infer bulk properties of QGP.

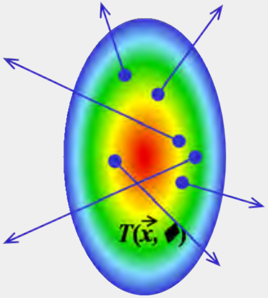

- High energy particles lose energy when they traverse QGP.
- This energy loss is sensitive to QGP properties.
- We can realistically predict this energy loss.

- High-$p_\perp$ probes are excellent tomoraphy tools.
- We can use them to infer some of the bulk QGP properties.

How to infer the shape of the QGP droplet from the data?

- Initial spatial anisotropy is one of the main properties of QGP.
- A major limiting factor for QGP tomography.

- Initial spatial anisotropy is one of the main properties of QGP.
- A major limiting factor for QGP tomography.
- Still not possible to directly infer the initial anisotropy from experimental data.

Shape of the QGP droplet

- Initial spatial anisotropy is one of the main properties of QGP.
- A major limiting factor for QGP tomography.
- Still not possible to directly infer the initial anisotropy from experimental data.
- Several theoretical studies (MC-Glauber, EKRT, IP-Glasma, MC-KLN) infer the initial anisotropy; lead to notably different predictions.

Shape of the QGP droplet

- Initial spatial anisotropy is one of the main properties of QGP.
- A major limiting factor for QGP tomography.
- Still not possible to directly infer the initial anisotropy from experimental data.
- Several theoretical studies (MC-Glauber, EKRT, IP-Glasma, MC-KLN) infer the initial anisotropy; lead to notably different predictions.

⬇

- Alternative approaches for inferring anisotropy are necessary!

Shape of the QGP droplet

- Initial spatial anisotropy is one of the main properties of QGP.
- A major limiting factor for QGP tomography.
- Still not possible to directly infer the initial anisotropy from experimental data.
- Several theoretical studies (MC-Glauber, EKRT, IP-Glasma, MC-KLN) infer the initial anisotropy; lead to notably different predictions.

⬇

- Alternative approaches for inferring anisotropy are necessary!
- Optimally, these should be complementary to existing predictions.

Shape of the QGP droplet

- Initial spatial anisotropy is one of the main properties of QGP.
- A major limiting factor for QGP tomography.
- Still not possible to directly infer the initial anisotropy from experimental data.
- Several theoretical studies (MC-Glauber, EKRT, IP-Glasma, MC-KLN) infer the initial anisotropy; lead to notably different predictions.

$\Downarrow$

- Alternative approaches for inferring anisotropy are necessary!
- Optimally, these should be complementary to existing predictions.
- Based on a method that is fundamentally different than models of early stages of QCD matter.

- Inference from already available high-$p_\perp$ R_{AA} and v_2 measurements (to be measured with higher precision in the future).

- Inference from already available high-$p_\perp$ R_{AA} and v_2 measurements (to be measured with higher precision in the future).
- Use experimental data (rather than calculations which rely on early stages of QCD matter).
- Exploit information from interactions of rare high-$p_\perp$ partons with QCD medium.

- Inference from already available high-$p_\perp$ R_{AA} and v_2 measurements (to be measured with higher precision in the future).

- Use experimental data (rather than calculations which rely on early stages of QCD matter).
- Exploit information from interactions of rare high-$p_\perp$ partons with QCD medium.

- Advances the applicability of high-$p_\perp$ data.
- Up to now, this data was mainly used to study the jet-medium interacions, rather than inferring bulk QGP parameters, such as spatial anisotropy.

What is an appropriate observable?

The initial state anisotropy is quantified in terms of eccentricity parameter ϵ_2:

$$\epsilon_2 = \frac{\langle y^2 - x^2 \rangle}{\langle y^2 + x^2 \rangle} = \frac{\int dx\, dy\, (y^2 - x^2)\, \rho(x, y)}{\int dx\, dy\, (y^2 + x^2)\, \rho(x, y)},$$

where $\rho(x, y)$ is the initial density distribution of the QGP droplet.

M. Djordjevic, S. Stojku, M. Djordjevic and P. Huovinen, Phys.Rev. C Rapid Commun. 100, 031901 (2019).

What is an appropriate observable?

The initial state anisotropy is quantified in terms of eccentricity parameter ϵ_2:

$$\epsilon_2 = \frac{\langle y^2 - x^2 \rangle}{\langle y^2 + x^2 \rangle} = \frac{\int dx\, dy\, (y^2 - x^2)\, \rho(x, y)}{\int dx\, dy\, (y^2 + x^2)\, \rho(x, y)},$$

where $\rho(x, y)$ is the initial density distribution of the QGP droplet.

M. Djordjevic, S. Stojku, M. Djordjevic and P. Huovinen, Phys.Rev. C Rapid Commun. 100, 031901 (2019).

- High-$p_\perp$ v_2 is sensitive to both the anisotropy and the size of the system.
- R_{AA} is sensitive only to the size of the system.

What is an appropriate observable?

The initial state anisotropy is quantified in terms of eccentricity parameter ϵ_2:

$$\epsilon_2 = \frac{\langle y^2 - x^2 \rangle}{\langle y^2 + x^2 \rangle} = \frac{\int dx\, dy\, (y^2 - x^2)\, \rho(x, y)}{\int dx\, dy\, (y^2 + x^2)\, \rho(x, y)},$$

where $\rho(x, y)$ is the initial density distribution of the QGP droplet.

M. Djordjevic, S. Stojku, M. Djordjevic and P. Huovinen, Phys.Rev. C Rapid Commun. 100, 031901 (2019).

- High-$p_\perp$ v_2 is sensitive to both the anisotropy and the size of the system.
- R_{AA} is sensitive only to the size of the system.

⬇

Can we extract eccentricity from high-$p_\perp$ R_{AA} and v_2?

Use scaling arguments for high-$p_\perp$

$\Delta E/E \approx \langle T\rangle^a \langle L\rangle^b$, where within our model $a \approx 1.2$, $b \approx 1.4$

D. Zigic *et al.*, JPG 46, 085101 (2019); M. Djordjevic and M. Djordjevic, PRC 92, 024918 (2015)

Use scaling arguments for high-$p_\perp$

$\Delta E/E \approx \langle T\rangle^a \langle L\rangle^b$, where within our model $a \approx 1.2$, $b \approx 1.4$

D. Zigic *et al.*, JPG 46, 085101 (2019); M. Djordjevic and M. Djordjevic, PRC 92, 024918 (2015)

$$R_{AA} \approx 1 - \xi \langle T\rangle^a \langle L\rangle^b$$

$$1 - R_{AA} \approx \xi \langle T\rangle^a \langle L\rangle^b$$

$$v_2 \approx \frac{1}{2} \frac{R_{AA}^{in} - R_{AA}^{out}}{R_{AA}^{in} + R_{AA}^{out}} \Longrightarrow$$

$$v_2 \approx \xi \langle T\rangle^a \langle L\rangle^b \left(\frac{b}{2} \frac{\Delta L}{\langle L\rangle} - \frac{a}{2} \frac{\Delta T}{\langle T\rangle} \right)$$

Anisotropy observable

Use scaling arguments for high-$p_\perp$

$\Delta E/E \approx \langle T\rangle^a \langle L\rangle^b$, where within our model $a \approx 1.2$, $b \approx 1.4$

D. Zigic *et al.*, JPG 46, 085101 (2019); M. Djordjevic and M. Djordjevic, PRC 92, 024918 (2015)

$$R_{AA} \approx 1 - \xi \langle T\rangle^a \langle L\rangle^b$$

$$1 - R_{AA} \approx \xi \langle T\rangle^a \langle L\rangle^b$$

$$v_2 \approx \frac{1}{2}\frac{R_{AA}^{in} - R_{AA}^{out}}{R_{AA}^{in} + R_{AA}^{out}} \Longrightarrow$$

$$v_2 \approx \xi \langle T\rangle^a \langle L\rangle^b \left(\frac{b}{2}\frac{\Delta L}{\langle L\rangle} - \frac{a}{2}\frac{\Delta T}{\langle T\rangle}\right)$$

$$\Downarrow$$

$$\boxed{\frac{v_2}{1 - R_{AA}} \approx \left(\frac{b}{2}\frac{\Delta L}{\langle L\rangle} - \frac{a}{2}\frac{\Delta T}{\langle T\rangle}\right)}$$

This ratio carries information on the asymmetry of the system, but through both spatial and temperature variables.

M. Djordjevic, S. Stojku, M. Djordjevic and P. Huovinen, Phys.Rev. C Rapid Commun. 100, 031901 (2019).

Temperature vs. spatial asymmetry:

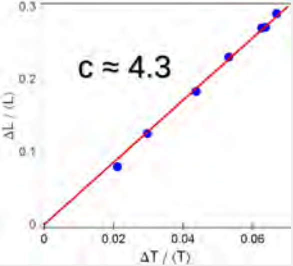

$$\frac{v_2}{1 - R_{AA}} \approx \left(\frac{b}{2} \frac{\Delta L}{\langle L \rangle} - \frac{a}{2} \frac{\Delta T}{\langle T \rangle} \right) \Longrightarrow$$

Anisotropy parameter ς

Temperature vs. spatial asymmetry:

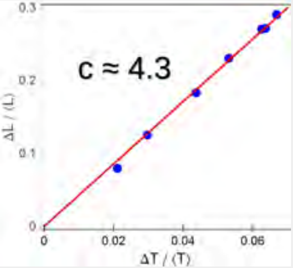

$$\frac{v_2}{1-R_{AA}} \approx \left(\frac{b}{2}\frac{\Delta L}{\langle L\rangle} - \frac{a}{2}\frac{\Delta T}{\langle T\rangle}\right) \Longrightarrow$$

$$\boxed{\frac{v_2}{1-R_{AA}} \approx \frac{1}{2}\left(b-\frac{a}{c}\right)\frac{\langle L_{out}\rangle - \langle L_{in}\rangle}{\langle L_{out}\rangle + \langle L_{in}\rangle} \approx 0.57\varsigma}$$

$$\boxed{\varsigma = \frac{\Delta L}{\langle L\rangle} = \frac{\langle L_{out}\rangle - \langle L_{in}\rangle}{\langle L_{out}\rangle + \langle L_{in}\rangle}}$$

Temperature vs. spatial asymmetry:

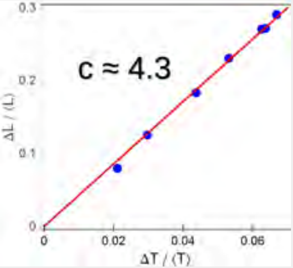

$$\frac{v_2}{1-R_{AA}} \approx \left(\frac{b}{2}\frac{\Delta L}{\langle L\rangle} - \frac{a}{2}\frac{\Delta T}{\langle T\rangle}\right) \Longrightarrow$$

$$\boxed{\frac{v_2}{1-R_{AA}} \approx \frac{1}{2}\left(b-\frac{a}{c}\right)\frac{\langle L_{out}\rangle - \langle L_{in}\rangle}{\langle L_{out}\rangle + \langle L_{in}\rangle} \approx 0.57\varsigma}$$

$$\boxed{\varsigma = \frac{\Delta L}{\langle L\rangle} = \frac{\langle L_{out}\rangle - \langle L_{in}\rangle}{\langle L_{out}\rangle + \langle L_{in}\rangle}}$$

- At high $p_\perp$, v_2 over $1-R_{AA}$ ratio is dictated *solely* by the geometry of the initial fireball!
- Anisotropy parameter ς follows directly from high $p_\perp$ experimental data!

M. Djordjevic, S. Stojku, M. Djordjevic and P. Huovinen, Phys.Rev. C Rapid Commun. 100, 031901 (2019).

Comparison with experimental data

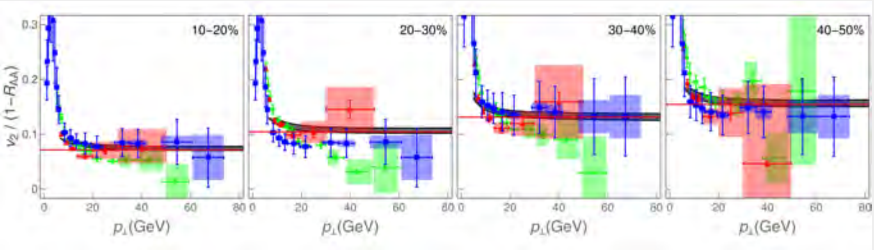

- Solid red line: analytically derived asymptote.

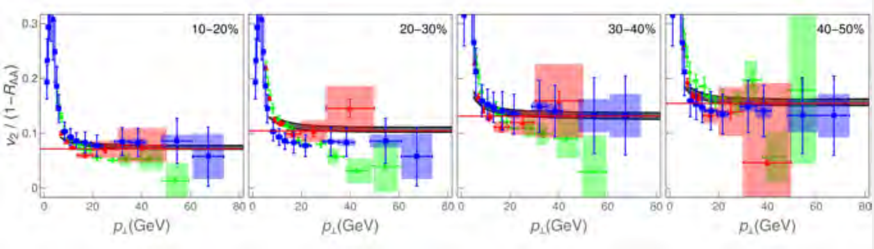

- Solid red line: analytically derived asymptote.
- For each centrality and from $p_\perp \approx 20 GeV$, $v_2/(1-R_{AA})$ does not depend on $p_\perp$, but is determined by the geometry of the system.

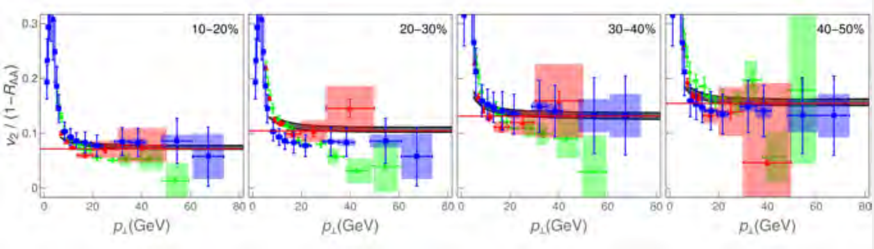

- Solid red line: analytically derived asymptote.
- For each centrality and from $p_\perp \approx 20GeV$, $v_2/(1-R_{AA})$ does not depend on $p_\perp$, but is determined by the geometry of the system.
- The experimental data from ALICE, CMS and ATLAS show the same tendency, though the error bars are still large.
- In the LHC Run 3 the error bars should be significantly reduced.

Comparison with experimental data

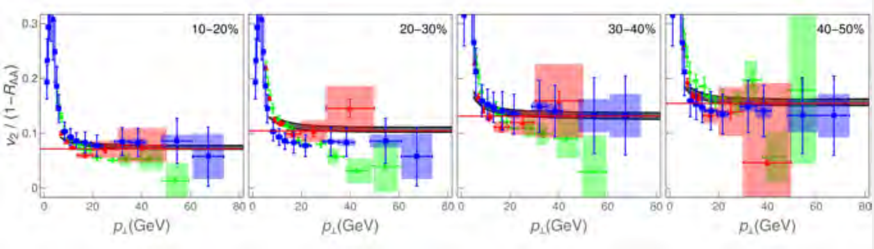

- $v_2/(1-R_{AA})$ indeed carries the information about the system's anisotropy.
- It can be simply (from the straight line high-$p_\perp$ limit) and robustly (in the same way for each centrality) inferred from experimental data.

Eccentricity

Anisotropy parameter ς is not the commonly used anisotropy parameter ϵ_2. To facilitate comparison with ϵ_2 values in the literature, we define:

$$\epsilon_{2L} = \frac{\langle L_{out} \rangle^2 - \langle L_{in} \rangle^2}{\langle L_{out} \rangle^2 + \langle L_{in} \rangle^2} = \frac{2\varsigma}{1+\varsigma^2} \implies$$

M. Djordjevic, S. Stojku, M. Djordjevic and P. Huovinen, Phys.Rev. C Rapid Commun. 100, 031901 (2019).

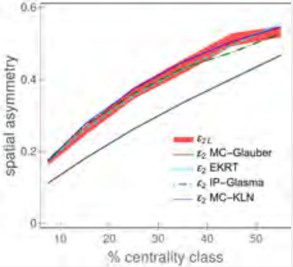

Eccentricity

Anisotropy parameter ς is not the commonly used anisotropy parameter ϵ_2. To facilitate comparison with ϵ_2 values in the literature, we define:

$$\epsilon_{2L} = \frac{\langle L_{out}\rangle^2 - \langle L_{in}\rangle^2}{\langle L_{out}\rangle^2 + \langle L_{in}\rangle^2} = \frac{2\varsigma}{1+\varsigma^2} \implies$$

M. Djordjevic, S. Stojku, M. Djordjevic and P. Huovinen, Phys.Rev. C Rapid Commun. 100, 031901 (2019).

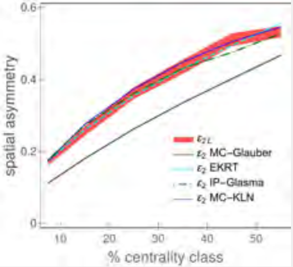

ϵ_{2L} is in an excellent agreement with ϵ_2 which we started from.

$v_2/(1-R_{AA})$ provides a reliable and robust procedure to recover initial state anisotropy.

ECCENTRICITY

Anisotropy parameter ς is not the commonly used anisotropy parameter ϵ_2. To facilitate comparison with ϵ_2 values in the literature, we define:

$$\epsilon_{2L} = \frac{\langle L_{out}\rangle^2 - \langle L_{in}\rangle^2}{\langle L_{out}\rangle^2 + \langle L_{in}\rangle^2} = \frac{2\varsigma}{1+\varsigma^2} \implies$$

M. Djordjevic, S. Stojku, M. Djordjevic and P. Huovinen, Phys.Rev. C Rapid Commun. 100, 031901 (2019).

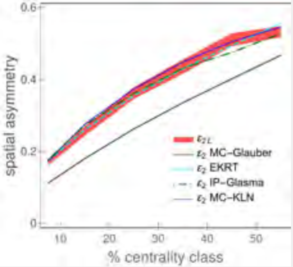

ϵ_{2L} is in an excellent agreement with ϵ_2 which we started from.

$v_2/(1-R_{AA})$ provides a reliable and robust procedure to recover initial state anisotropy.

The width of our ϵ_{2L} band is smaller than the difference in ϵ_2 values obtained by using different models.

Resolving power to distinguish between different initial state models, although it may not be possible to separate the finer details of more sophisticated models.

Summary

- High-$p_\perp$ theory and data - traditionally used to explore high-$p_\perp$ parton interactions with QGP, while QGP properties are explored through low-$p_\perp$ data and corresponding models.

Summary

- High-$p_\perp$ theory and data - traditionally used to explore high-$p_\perp$ parton interactions with QGP, while QGP properties are explored through low-$p_\perp$ data and corresponding models.
- With a proper description of high-$p_\perp$ medium interactions, high-$p_\perp$ probes can become powerful tomography tools, as they are sensitive to global QGP properties. We showed that here in the case of spatial anisotropy of QCD matter.

Summary

- High-$p_\perp$ theory and data - traditionally used to explore high-$p_\perp$ parton interactions with QGP, while QGP properties are explored through low-$p_\perp$ data and corresponding models.
- With a proper description of high-$p_\perp$ medium interactions, high-$p_\perp$ probes can become powerful tomography tools, as they are sensitive to global QGP properties. We showed that here in the case of spatial anisotropy of QCD matter.
- By using our dynamical energy loss formalism, we showed that a (modified) ratio of R_{AA} and v_2 presents a reliable and robust observable for straightforward extraction of initial state anisotropy.

Summary

- High-$p_\perp$ theory and data - traditionally used to explore high-$p_\perp$ parton interactions with QGP, while QGP properties are explored through low-$p_\perp$ data and corresponding models.
- With a proper description of high-$p_\perp$ medium interactions, high-$p_\perp$ probes can become powerful tomography tools, as they are sensitive to global QGP properties. We showed that here in the case of spatial anisotropy of QCD matter.
- By using our dynamical energy loss formalism, we showed that a (modified) ratio of R_{AA} and v_2 presents a reliable and robust observable for straightforward extraction of initial state anisotropy.
- It will be possible to infer anisotropy directly from LHC Run 3 data: an important constraint to models describing the early stages of QGP formation. This demonstates the synergy of more common approaches for inferring QGP properties with high-$p_\perp$ theory and data.

Acknowledgements

European Research Council

Established by the European Commission

МИНИСТАРСТВО ПРОСВЕТЕ,
НАУКЕ И ТЕХНОЛОШКОГ РАЗВОЈА

The speaker has received funding from the European Research Council (ERC) under the European Union's Horizon 2020 research and innovation programme (grant agreement No 725741)

$v2/(1 - R_{AA})$ with full 3+1D hydro DREENA

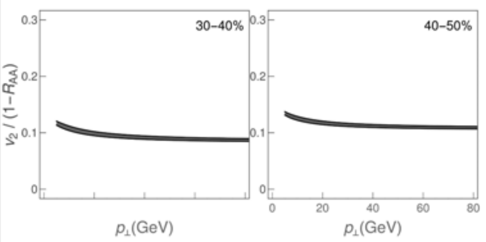

Flatness still observed. Further research is ongoing.

Accelerating longitudinal expansion of resistive relativistic-magneto-hydrodynamics

M. Haddadi Moghaddam
In Collaboration with: W. M. Alberico, Duan She

Universita degli Studi di Torino
INFN sezione di Torino

Frontiers in Nuclear and Hadronic Physics 2020
GGI, Florence, Italy

Feb 24 - March 06

Overview

1. Relativistic Magneto-hydrodynamics in heavy ion collisions(RMHD)
2. Accelerating Longitudinal fluid
3. Results and discussion

RRMHD

RMHD equations

The coupled RMHD equations are

$$d_\mu T^{\mu\nu} = 0, \quad T^{\mu\nu} = T^{\mu\nu}_{matt} + T^{\mu\nu}_{EM}$$
$$d_\mu F^{\mu\nu} = -J^\nu, \quad (d_\mu J^\mu = 0), \; J^\mu = \rho u^\mu + \sigma^{\mu\nu} e_\nu$$
$$d_\mu F^{*\mu\nu} = 0, \; e^\mu = F^{\mu\nu} u_\nu, \; b^\mu = F^{*\mu\nu} u_\nu$$

Where ρ(Here is zero) is electric charge density. Note that d_μ is covariant derivative .

In the case of finite and homogeneous electrical conductivity $\sigma^{ij} = \sigma\delta^{ij}$,

For the Resistive RMHD we can re-write the energy and Euler equations as follow:

$$D\epsilon + (\epsilon + P)\Theta = e^\lambda J_\lambda, \; (D = u^\mu d_\mu, \Theta = d_\mu u^\mu),$$
$$(\epsilon + P)Du^\alpha + \nabla^\alpha P = F^{\alpha\lambda} J_\lambda - u^\alpha e^\lambda J_\lambda.$$

RMHD

Ideal RMHD in magnetized Bjorken model

$$\text{In co-moving frame}: u^{\mu} = (1,0,0,0) \tag{1}$$

And one assume magnetic field is located in the transverse direction

$$b^{\mu} = (0, b^{x}, b^{y}, 0) \tag{2}$$

According to Bjorken flow $(v_z = \frac{z}{t})$ $D = \partial_\tau,\ \Theta = \frac{1}{\tau}$. Finally energy density and magnetic field are given by

$$\epsilon(\tau) = \frac{\epsilon_c}{\tau^{4/3}}, \quad b(\tau) = b_0(\frac{\tau_0}{\tau}) \tag{3}$$

V. Roy et al, Phys. Lett. B, Vol. 750, (2015)
Gabriele Inghirami et al, Eur. Phys. J. C (2016) 76:659.
M. Haddadi Moghaddam et al, Eur. Phys. J. C (2018) 78:255.

(1+1)D Longitudinal expansion with acceleration

We can parameterize the fluid four-velocity in (1+1)D as follows

$$u^\mu = \gamma(1, 0, 0, v_z) = (\cosh Y, 0, 0, \sinh Y), \tag{4}$$

where Y is the fluid rapidity and $v_z = \tanh Y$. Besides, in Milne coordinates (τ, x, y, η), one can write

$$u^\mu = \left[\cosh(Y-\eta), 0, 0, \frac{1}{\tau}\sinh(Y-\eta)\right] = \bar{\gamma}[1, 0, 0, \frac{1}{\tau}\bar{v}], \tag{5}$$

where

$$\bar{\gamma} = \cosh(Y-\eta), \;\; \bar{v} = \tanh(Y-\eta). \tag{6}$$

By using this parameterization one obtains

$$D = \bar{\gamma}(\partial_\tau + \frac{1}{\tau}\bar{v}\partial_\eta) \tag{7}$$

$$\Theta = \bar{\gamma}(\bar{v}\partial_\tau Y + \frac{1}{\tau}\partial_\eta Y) \tag{8}$$

(1+1)D Longitudinal expansion with acceleration

Non central collisions can create an out-of-plane magnetic field and in-plane electric field. The magnetic field in non central collisions is dominated by the y component which induces a Faraday current in xz plane. We consider the following setup:

$$u^\mu = \bar{\gamma}[1, 0, 0, \frac{1}{\tau}\bar{v}],$$
$$e^\mu = [0, e^x, 0, 0],$$
$$b^\mu = [0, 0, b^y, 0].$$

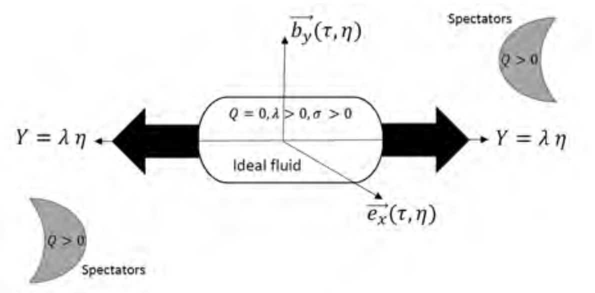

Figure: λ is acceleration parameter.

(1+1D) Longitudinal expansion with acceleration

We summarize the RRMHD align in (1+1D):

$$(\tau\partial_\tau + \bar{v}\partial_\eta)\epsilon + (\epsilon + P)(\tau\bar{v}\partial_\tau Y + \partial_\eta Y) = \bar{\gamma}^{(-1)}\tau\sigma\ e_x^2,$$

$$(\epsilon + P)(\tau\partial_\tau + \bar{v}\partial_\eta)Y + (\tau\bar{v}\partial_\tau + \partial_\eta)P = \bar{\gamma}^{(-1)}\tau\sigma\ e^x b^y,$$

$$\partial_\tau(u^\tau b^y + \frac{1}{\tau}e_x u_\eta) + \partial_\eta(u^\eta b^y - \frac{1}{\tau}e_x u_\tau) + (\frac{1}{\tau})(u^\tau b^y + \frac{1}{\tau}e_x u_\eta) = 0,$$

$$\partial_\tau(u^\tau e^x + (\frac{1}{\tau})b_y u_\eta) + \partial_\eta(u^\eta e^x - \frac{1}{\tau}b_y u_\tau) + (\frac{1}{\tau})(u^\tau e^x + (\frac{1}{\tau})b_y u_\eta) = -\sigma e_x.$$

We suppose that all quantities are constant in the transverse plane. Hence in order to solve the last two equations, we can write the following Ansatz:

$$e_x(\tau,\eta) = -h(\tau,\eta)\sinh(Y-\eta) \tag{9}$$
$$b_y(\tau,\eta) = h(\tau,\eta)\cosh(Y-\eta) \tag{10}$$

then we have:

$$\partial_\tau h(\tau,\eta) + \frac{h(\tau,\eta)}{\tau} = 0, \tag{11}$$
$$\partial_\eta h(\tau,\eta) + (\sigma\tau)h(\tau,\eta)\sinh(\eta - Y) = 0 \tag{12}$$

and the solutions of the above Equations can be written as:

$$h(\tau,\eta) = \frac{c(\eta)}{\tau}, \tag{13}$$
$$\sinh(Y-\eta) = \frac{1}{\sigma\tau}\frac{\partial_\eta c(\eta)}{c(\eta)}, \tag{14}$$
$$\cosh(Y-\eta) = \sqrt{1+\frac{1}{\sigma^2\tau^2}(\frac{\partial_\eta c(\eta)}{c(\eta)})^2} \tag{15}$$

Analytical Solutions

We summarize the solutions for fluid rapidity, four velocity profile and EM fields as follows:

$$Y = \eta + \sinh^{-1}\left(\frac{1}{\sigma\tau}\frac{\partial_\eta c(\eta)}{c(\eta)}\right), \quad (16)$$

$$u^\tau = \sqrt{1 + \frac{1}{\sigma^2\tau^2}\left(\frac{\partial_\eta c(\eta)}{c(\eta)}\right)^2}, \quad (17)$$

$$u^\eta = \frac{1}{\sigma\tau^2}\frac{\partial_\eta c(\eta)}{c(\eta)}, \quad (18)$$

$$e_x(\tau, \eta) = -\frac{1}{\sigma\tau^2}\frac{\partial c(\eta)}{\partial\eta}, \quad (19)$$

$$b_y(\tau, \eta) = \frac{c(\eta)}{\tau} \times \sqrt{1 + \frac{1}{\sigma^2\tau^2}\left(\frac{\partial_\eta c(\eta)}{c(\eta)}\right)^2}. \quad (20)$$

The energy and momentum conservation equations are solved numerically.

Definition of function $c(\eta)$?

converting of the EM fields from Milne to Cartesian coordinates in the lab frame:

$$\mathbf{E}_L = (\sinh(\eta)\frac{c(\eta)}{\tau}, 0, 0), \tag{21}$$

$$\mathbf{B}_L = (0, \cosh(\eta)\frac{c(\eta)}{\tau}, 0) \tag{22}$$

Observation:
Where $c(\eta) = c_0(1 + \frac{\alpha^2}{2!}\eta^2 + ...)$ is considered. If we choose a constant value for $c(\eta) =$const, then the flow has no acceleration $\lambda = 1$, $(Y \equiv \eta \to \bar{v} = 0)$, the electric field in co-moving frame e_x vanishes and we have: $b_y \propto \frac{1}{\tau}$, $\epsilon \propto \tau^{-\frac{4}{3}}$ if $c_s^2 = \frac{1}{3}$.

Initial Condition for Magnetic field

In order to fix the constant, c_0, the initial condition for magnetic field at mid rapidity in the lab frame is considered $eB_L^y(\tau_0 = 0.5, 0) = 0.0018 GeV^2$, and coefficient α is selected in order to parameterize the acceleration λ.

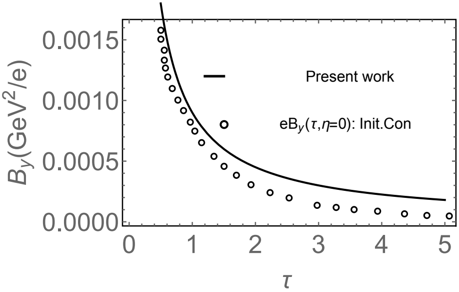

Figure: Magnetic field B_y at mid-rapidity in the lab frame.

U. Gürsoy, et al. Phys. Rev. C **98**, 055201 (2018).

Longitudinal acceleration λ

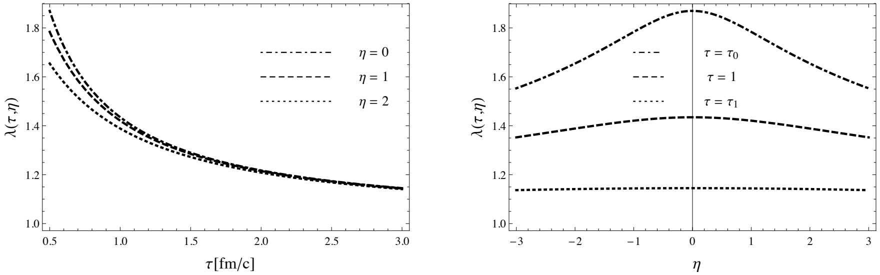

Figure: Acceleration parameter $\lambda(\tau, \eta)$ in term of proper time τ (Left) and rapidity η (Right). The coefficients are chosen for $\alpha = 0.1, \ \sigma = 0.023 \ fm^{-1}$.

At the late time of the expansion $\lambda \to 1$ and in the both forward and backward rapidity, by increasing the rapidity, the acceleration parameter decreases.

Dynamical evolution of electric field e_x

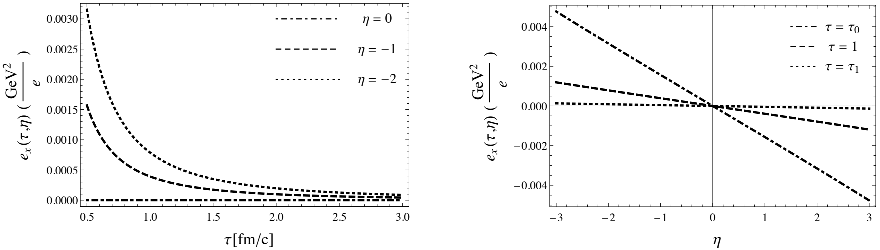

Figure: Electric field $e_x(\tau, \eta)$ in term of proper time τ (Left) and rapidity η (Right). The coefficients are chosen for $\alpha = 0.1$, $\sigma = 0.023$ fm^{-1}.

Dynamical evolution of magnetic field b_y

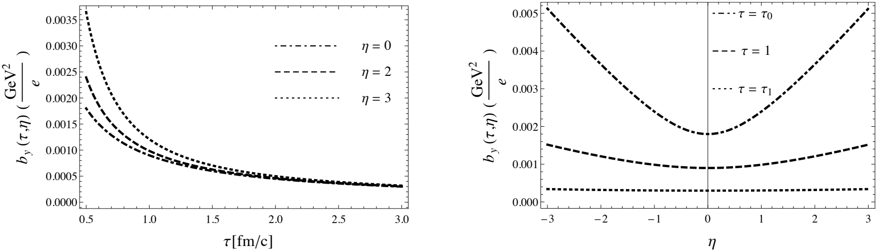

Figure: Magnetic field $e_x(\tau, \eta)$ in term of proper time τ (Left) and rapidity η (Right). The coefficients are chosen for $\alpha = 0.1,\ \sigma = 0.023\ fm^{-1}$.

The energy density ϵ of the magnetized matter

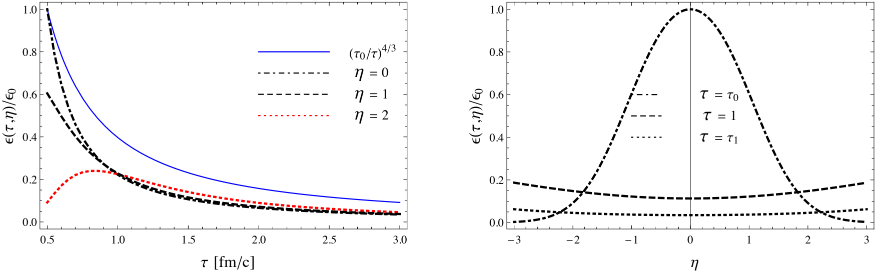

Figure: The ratio of energy density $\epsilon(\tau, \eta)/\epsilon_0$ in term of proper time τ (Left) and rapidity η (Right). The coefficients are chosen for $\alpha = 0.1$, $\sigma = 0.023$ fm^{-1}.

Observation

K.J. Eskola and et al, Eur. Phys. J. C 1, 627-632 (1998).
P. Bozek, Phys. Rev. C 77, 034911 (2008).

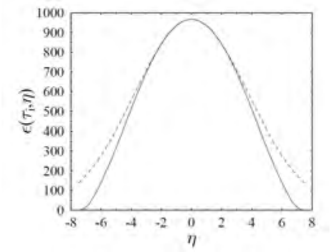

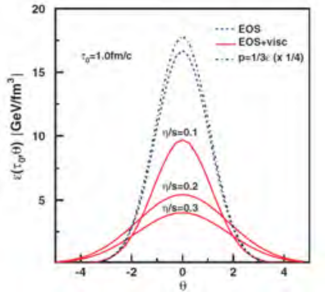

Figure: (Left): The initial energy condition for $\epsilon(\tau_0, \eta)$ for $\sqrt{s} = 5500$ GeV. The dashed curve is Gaussian fit $\epsilon(\tau_0, \eta) = \epsilon_0 \exp\left(-\frac{\eta^2}{2w^2}\right)$, with $w = 3.8$. (Right): Initial energy density distribution for the ideal fluid hydrodynamic evolution with a realistic EOS (dashed line), for viscous hydrodynamic evolutions (solid lines), and for a relativistic gas EOS (dashed-dotted line).

Connection between energy density and electrical conductivity

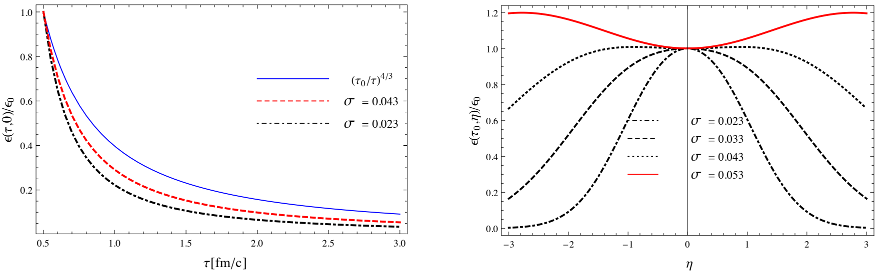

Figure: The ratio of energy density $\epsilon(\tau,\eta)/\epsilon_0$ in term of proper time τ (Left) and rapidity η (Right). The coefficients are chosen for $\alpha = 0.1$.

It seems that there is a critical upper bound for the electrical conductivity of the matter:

$$\sigma < 0.053 \ fm^{-1}$$

Connection between energy density and parameter α

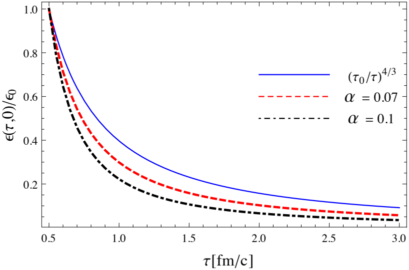

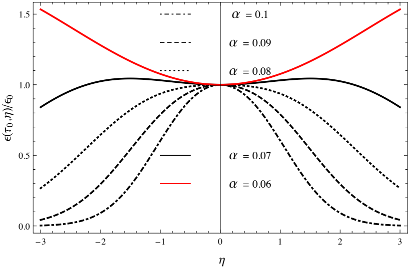

Figure: The ratio of energy density $\epsilon(\tau,\eta)/\epsilon_0$ in term of proper time τ (Left) and rapidity η (Right). The coefficients are chosen for $\alpha = 0.1$.

It seems that there is a critical lower bound for α:

$$\alpha > 0.06$$

Thank You

Backup Slides

Relativistic MHD

Energy-momentum tensor and four vector fields

$$T_{pl}^{\mu\nu} = (\epsilon + P)u^\mu u^\nu + Pg^{\mu\nu} \quad (23)$$

$$T_{em}^{\mu\nu} = F^{\mu\eta}F_\eta^{\ \nu} - \frac{1}{4}F^{\eta\rho}F_{\eta\rho}g^{\mu\nu} \quad (24)$$

$$F^{\mu\nu} = u^\mu e^\nu - u^\nu e^\mu + \varepsilon^{\mu\nu\lambda\kappa}b_\lambda u_\kappa, \quad (25)$$

$$F^{\star\alpha\beta} = u^\mu b^\nu - u^\nu b^\mu - \varepsilon^{\mu\nu\lambda\kappa}e_\lambda u_\kappa \quad (26)$$

$$\text{Levi - Civita} : \varepsilon^{\mu\nu\lambda\kappa} = 1/\sqrt{-\det g}[\mu\nu\lambda\kappa], \quad (27)$$

$$\text{Electric four vector} : e^\alpha = \gamma[\mathbf{v}\cdot\mathbf{E}, (\mathbf{E} + \mathbf{v}\times\mathbf{B})]^T, (\mathrm{Cartesian}) \quad (28)$$

$$\text{Magnetic four vector} : b^\alpha = \gamma[\mathbf{v}\cdot\mathbf{B}, (\mathbf{B} - \mathbf{v}\times\mathbf{E})]^T, (\mathrm{Cartesian}) \quad (29)$$

Where $\vec{v}, \vec{B}, \vec{E}$ are measured in lab frame and γ is Lorentz factor.

Why to study magnetic field in HIC?

Strong magnetic field may produce many effects:

1. The Chiral Magnetic Effect (CME)
2. The Chiral Magnetic Wave (CMW)
3. The Chiral separation Hall effect (CSHE)
4. Influence on the elliptic flow (v_2)
5. Influence on the directed flow (v_1)
6. ...

Diffusion of heavy quarks in the early stage of high energy nuclear collisions

Junhong Liu[12]

in collaboration with S. Plumari, S. K. Das, V. Greco, and M. Ruggieri

[1]School of Nuclear Science and Technology, Lanzhou University

[2]INFN-Laboratori Nazionali del Sud

Florence Italy, February 2020

Table of Contents

1 High energy nuclear collisions

2 Classical Yang-Mills fields

3 Diffusion of heavy quark in glasma

4 Summary

Table of Contents

1 High energy nuclear collisions

2 Classical Yang-Mills fields

3 Diffusion of heavy quark in glasma

4 Summary

Relativistic Heavy Ion Collisions

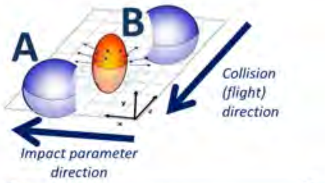

A,B: Cu, Au (RHIC@BNL)
Pb (LHC@CERN)
p (LHC@CERN)
p-Pb collisions (LHC@CERN)
d-Au collisions (RHIC@BNL)

$\mathrm{Au-Au}: \sqrt{s} = 200 \times A\ \mathrm{GeV}$ at RHIC
$\mathrm{Pb-Pb}: \sqrt{s} = 2.76 \times A\ \mathrm{TeV}$ at LHC
$\mathrm{p-Pb}: \sqrt{s} = 5.02\ \mathrm{TeV}$ at LHC
$\mathrm{p-p}: \sqrt{s} = 5,\ 7$ and $13\ \mathrm{TeV}$ at LHC

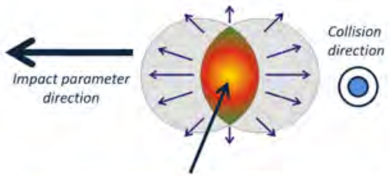

In Au-Au, Pb-Pb, Cu-Cu,......:
Hot and dense expanding
QUARK-GLUON-PLASMA (QGP)

QGP formation time
- RHIC 0.6 fm/c ≈ 10^{-24} sec
- LHC 0.2 fm/c

QGP lifetime
- RHIC 5 fm/c ≈ 10^{-23} sec
- LHC 10 fm/c

High energy nuclear collisions

Classical Yang-Mills fields

Diffusion of heavy quark in glasma

Summary

Collisions process

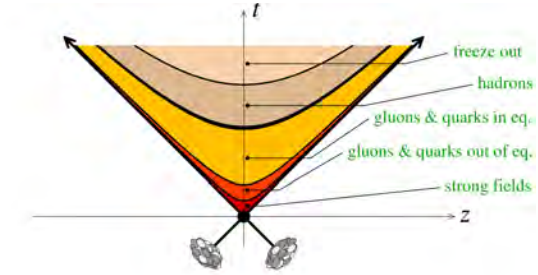

F. Gelis, Nucl.Phys. **A 854** (2011) 10-17

- initial stage: Glasma model
- QGP stage: transport theory
- Hadron stage: transport theory

Hybrid description of Relativistic Heavy Ion Collisions

Classical Yang-Mills field + Transport theory

Table of Contents

1 High energy nuclear collisions

2 Classical Yang-Mills fields

3 Diffusion of heavy quark in glasma

4 Summary

Initial condition

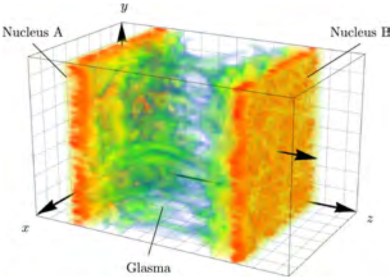

Andreas Ipp, David Müller Physics Letters B 771 (2017) 74-79

- Glasma can be treated as classical fields due to the large occupation number
- Initial glasma fields can be computed with the random static sources due to Lorentz time dilatation

$$\langle \rho^a(x_T)\rho^b(y_T)\rangle = (g^2\mu)^2\delta^{ab}\delta^{(2)}(x_T - y_T)$$

L. D. McLerran and R. Venugopalan, Phys. Rev. D 49, 2233 (1994)

Classical Yang-Mills fields

τ,η coordinates

$$\tau = \sqrt{t^2 - z^2} \qquad \eta = \frac{1}{2} ln \left[\frac{t+z}{t-z} \right]$$

In this case, CYM will be

$$\begin{aligned} E^i &= \tau \partial_\tau A_i, & (1) \\ E^\eta &= \frac{1}{\tau} \partial_\tau A_\eta, & (2) \\ \partial_\tau E^i &= \frac{1}{\tau} D_\eta F_{\eta i} + \tau D_j F_{ji}, & (3) \\ \partial_\tau E^\eta &= \frac{1}{\tau} D_j F_{j\eta}. & (4) \end{aligned}$$

Numerical results of CYM

Evolving fields up to 0.4 fm:

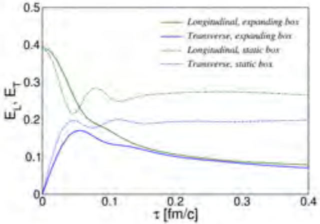

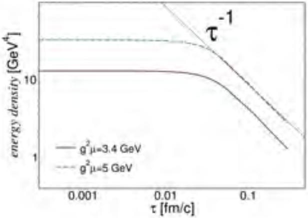

J. H. Liu, S. Plumari, S. K. Das, V. Greco, and M. Ruggieri 1911.02480

Table of Contents

1 High energy nuclear collisions

2 Classical Yang-Mills fields

3 Diffusion of heavy quark in glasma

4 Summary

heavy quarks as probes

- Carry negligible color current
- Self-interactions occur rarely
- Probe the very early evolution of the Glasma fields

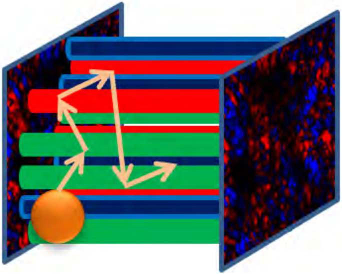

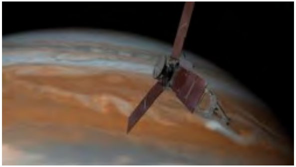

$$\frac{dx_i}{dt} = \frac{p_i}{E} \quad (5)$$

$$E\frac{dp_i}{dt} = Q_a F^a_{i\nu} p^\nu \quad (6)$$

$$E\frac{dQ_a}{dt} = Q_c \varepsilon^{cba} A_{b\mu} p^\mu \quad (7)$$

Spectrum of heavy quarks

M. Ruggieri and S. K. Das, Phys. Rev. D 98, no. 9, 094024 (2018)

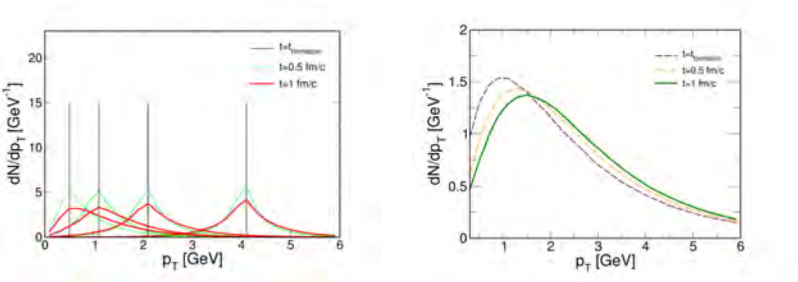

$$g^2\mu = 3.4GeV$$

Diffusion results in a shift of traverse momentum of heavy quarks.

RpA of heavy quarks

$$R_{pPb} = \frac{(dN/d^2P_T)_{final}}{(dN/d^2P_T)_{pQCD}} \qquad (8)$$

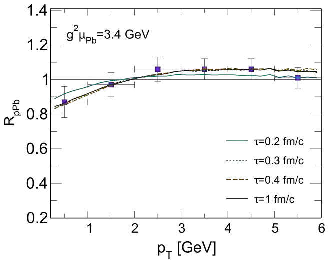

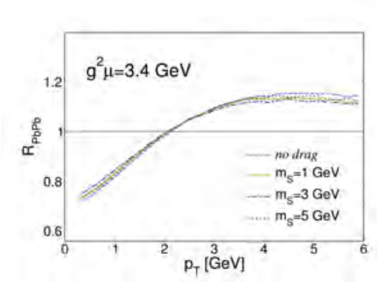

J. H. Liu, S. Plumari, S. K. Das, V. Greco, and M. Ruggieri 1911.02480

Table of Contents

1 High energy nuclear collisions

2 Classical Yang-Mills fields

3 Diffusion of heavy quark in glasma

4 Summary

Summary and future plan

- Borrowing the Glasma picture, the evolution of the system after the collision can be probed by heavy quarks observables
- The measured RpA can be understood as the diffusion of heavy quarks in the evolving Glasma
- $D\bar{D}$ correlation
- v1,v2,v3 of heavy quarks in the early stage

Summary and future plan

- Borrowing the Glasma picture, the evolution of the system after the collision can be probed by heavy quarks observables
- The measured RpA can be understood as the diffusion of heavy quarks in the evolving Glasma
- $D\bar{D}$ correlation
- v1,v2,v3 of heavy quarks in the early stage

Thank you!

Spin Hydrodynamics for the description of polarization of Lambda hyperons

Rajeev Singh

THE HENRYK NIEWODNICZAŃSKI INSTITUTE OF NUCLEAR PHYSICS POLISH ACADEMY OF SCIENCES

rajeev.singh@ifj.edu.pl

in collaboration with:
Wojciech Florkowski (IF UJ),
Radoslaw Ryblewski (IFJ PAN) and Avdhesh Kumar (NISER)

Primary References:

Phys. Rev. C 99, 044910 (2019)
Prog. Part. Nucl. Phys. 108 (2019) 103709

February 27, 2020
Frontiers in Nuclear and Hadronic Physics 2020
The GGI, Firenze, Italy

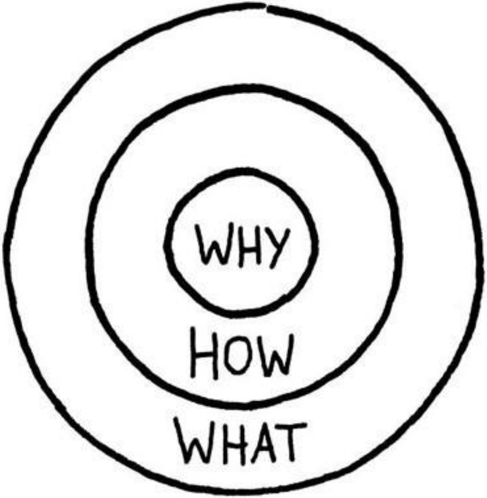
WHY
HOW
WHAT


WHY?

Motivation:

First positive measurements of global spin polarization of Λ hyperons by STAR

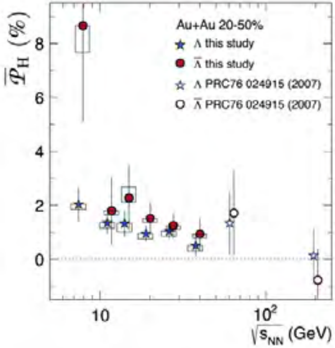

thermal approach $\longrightarrow$ $P_\Lambda \approx \frac{1}{2}\frac{\omega}{T} + \frac{\mu_\Lambda B}{T}$ $\quad P_{\bar{\Lambda}} \approx \frac{1}{2}\frac{\omega}{T} - \frac{\mu_\Lambda B}{T}$

Becattini, F., Karpenko, I., Lisa, M., Upsal, I., Voloshin, S., PRC 95, 054902 (2017)

... the hottest, least viscous – and now, most vortical – fluid produced in the laboratory ...

$$\omega = \left(P_\Lambda + P_{\bar{\Lambda}}\right) k_B T/\hbar \sim 0.6 - 2.7 \times 10^{22}\mathrm{s}^{-1}$$

L. Adamczyk et al. (STAR) (2017), Nature 548 (2017) 62-65

Motivation:

- Non-central relativistic heavy ion collisions creates global rotation of matter. This may induce spin polarization reminding us of Einstein and De-Haas effect and Barnett effect.

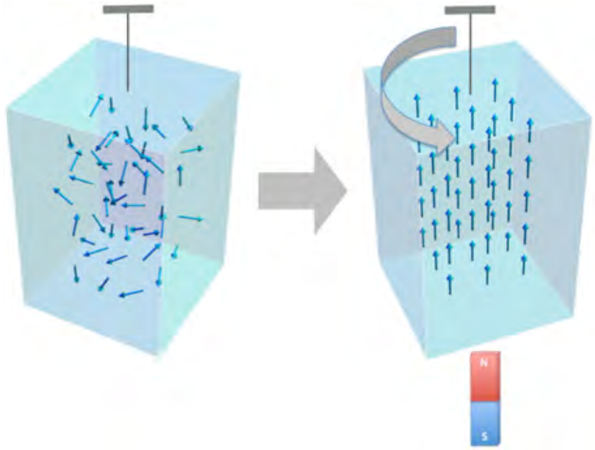

Figure: Einstein-De Haas Effect

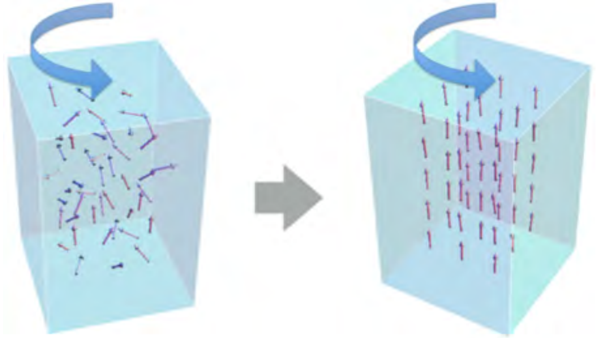

Figure: Barnett Effect

Motivation:

- Non-central relativistic heavy ion collisions creates global rotation of matter. This may induce spin polarization reminding us of Barnett effect and Einstein and de-Haas effect.
- Emerging particles are expected to be globally polarized with their spins on average pointing along the systems angular momentum.

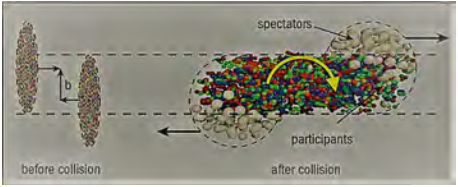

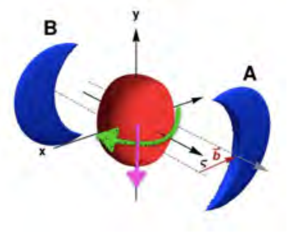

Figure: Schematic view of non-central heavy-ion collisions.

Source: CERN Courier

Other works:

- Other theoretical models used for the heavy-ions data interpretation dealt mainly with the spin polarization of particles at freeze-out, where the basic hydrodynamic quantity giving rise to spin polarization is the 'thermal vorticity' expressed as $\varpi_{\mu\nu} = -\frac{1}{2}(\partial_\mu \beta_\nu - \partial_\nu \beta_\mu)$.

F. Becattini *et.al.*(Annals Phys. 338 (2013)), F. Becattini, L. Csernai, D. J. Wang (PRC 88, 034905), F. Becattini *et.al.*(PRC 95, 054902), Iu. Karpenko, F. Becattini (EPJC (2017) 77: 213), F. Becattini, Iu. Karpenko(PRL 120, 012302 (2018))

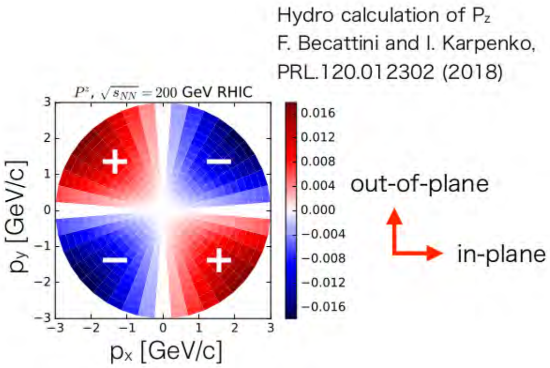


What?

Our hydrodynamic framework:

- Solving the standard perfect-fluid hydrodynamic equations without spin

Our hydrodynamic framework:

- Solving the standard perfect-fluid hydrodynamic equations without spin
- Determination of the spin evolution in the hydrodynamic background

Our hydrodynamic framework:

- Solving the standard perfect-fluid hydrodynamic equations without spin
- Determination of the spin evolution in the hydrodynamic background
- Determination of the Pauli-Lubanski (PL) vector on the freeze-out hypersurface

Our hydrodynamic framework:

- Solving the standard perfect-fluid hydrodynamic equations without spin.
- Determination of the spin evolution in the hydrodynamic background.
- Determination of the Pauli-Lubański (PL) vector on the freeze-out hypersurface.
- Calculation of the spin polarization of particles in their rest frame. The spin polarization obtained is a function of the three-momenta of particles and can be directly compared with the experiment.

Our hydrodynamic framework:

- In this work, we use relativistic hydrodynamic equations for polarized spin $1/2$ particles to determine the space-time evolution of the spin polarization in the system using forms of the energy-momentum and spin tensors proposed by de Groot, van Leeuwen, and van Weert (GLW).

  S. R. De Groot,Relativistic Kinetic Theory. Principles and Applications (1980).

Our hydrodynamic framework:

- In this work, we use relativistic hydrodynamic equations for polarized spin $1/2$ particles to determine the space-time evolution of the spin polarization in the system using forms of the energy-momentum and spin tensors proposed by de Groot, van Leeuwen, and van Weert (GLW).

  S. R. De Groot,Relativistic Kinetic Theory. Principles and Applications (1980).

- The calculations are done in a boost-invariant and transversely homogeneous setup. We show how the formalism of hydrodynamics with spin can be used to determine physical observables related to the spin polarization required for the modelling of the experimental data.

  Wojciech Florkowski *et.al.*(Phys. Rev. C 99, 044910), Wojciech Florkowski *et.al.*(Phys. Rev. C 97, 041901), Wojciech Florkowski *et.al.*(Phys. Rev. D 97, 116017).

Our hydrodynamic framework:

- In this work, we use relativistic hydrodynamic equations for polarized spin 1/2 particles to determine the space-time evolution of the spin polarization in the system using forms of the energy-momentum and spin tensors proposed by de Groot, van Leeuwen, and van Weert (GLW).

  S. R. De Groot,Relativistic Kinetic Theory. Principles and Applications (1980).

- The calculations are done in a boost-invariant and transversely homogeneous setup. We show how the formalism of hydrodynamics with spin can be used to determine physical observables related to the spin polarization required for the modelling of the experimental data.

  Wojciech Florkowski *et.al.*(Phys. Rev. C 99, 044910), Wojciech Florkowski *et.al.*(Phys. Rev. C 97, 041901), Wojciech Florkowski *et.al.*(Phys. Rev. D 97, 116017).

- Our hydrodynamic formulation does not allow for arbitrary large values of the spin polarization tensor, hence we have restricted ourselves to the leading order terms in the $\omega_{\mu\nu}$.


HOW ?
Paint X lite

Spin polarization tensor:

The spin polarization tensor $\omega_{\mu\nu}$ is anti-symmetric and can be defined by the four-vectors κ^{μ} and ω^{μ},

$$\omega_{\mu\nu} = \kappa_{\mu} U_{\nu} - \kappa_{\nu} U_{\mu} + \epsilon_{\mu\nu\alpha\beta} U^{\alpha} \omega^{\beta},$$

Note that, any part of the 4-vectors κ_{μ} and ω_{μ} which is parallel to U_{μ} does not contribute, therefore κ_{μ} and ω_{μ} satisfy the following orthogonality conditions:

$$\kappa \cdot U = 0, \quad \omega \cdot U = 0$$

We can express κ_{μ} and ω_{μ} in terms of $\omega_{\mu\nu}$, namely

$$\kappa_{\mu} = \omega_{\mu\alpha} U^{\alpha}, \quad \omega_{\mu} = \frac{1}{2} \epsilon_{\mu\alpha\beta\gamma} \omega^{\alpha\beta} U^{\gamma}$$

Conservation of charge:

$$\partial_\alpha N^\alpha(x) = 0,$$
$$\text{where,} \quad N^\alpha = nU^\alpha, \quad n = 4\sinh(\xi)\; n_{(0)}(T).$$

The quantity $n_{(0)}(T)$ defines the number density of spinless and neutral massive Boltzmann particles,

$$n_{(0)}(T) = \langle p \cdot U \rangle_0 = \frac{1}{2\pi^2}\, T^3\, \hat{m}^2 K_2\left(\hat{m}\right)$$

where, $\langle \cdots \rangle_0 \equiv \int dP \left(\cdots\right) e^{-\beta\cdot p}$ denotes the thermal average, $\hat{m} \equiv m/T$ denotes the ratio of the particle mass (m) and the temperature (T), and $K_2\left(\hat{m}\right)$ denotes the modified Bessel function.

The factor, $4\sinh(\xi) = 2\left(e^{\xi} - e^{-\xi}\right)$ accounts for spin degeneracy and presence of both particles and antiparticles in the system and the variable ξ denotes the ratio of the baryon chemical potential μ and the temperature T, $\xi = \mu/T$.

Conservation of energy and linear momentum:

$$\partial_\alpha T^{\alpha\beta}_{GLW}(x) = 0$$

where the energy-momentum tensor $T^{\alpha\beta}_{GLW}$ has the perfect-fluid form:

$$T^{\alpha\beta}_{GLW}(x) = (\varepsilon + P)U^\alpha U^\beta - P g^{\alpha\beta}$$

with energy density $\varepsilon = 4\cosh(\xi)\varepsilon_{(0)}(T)$ and pressure $P = 4\cosh(\xi)P_{(0)}(T)$

The auxiliary quantities are:

$\varepsilon_{(0)}(T) = \langle (p \cdot U)^2 \rangle_0$ and $P_{(0)}(T) = -(1/3)\langle p \cdot p - (p \cdot U)^2 \rangle_0$ are the energy density and pressure of the spin-less ideal gas respectively.

In case of ideal relativistic gas of classical massive particles,

$$\varepsilon_{(0)}(T) = \frac{1}{2\pi^2}\, T^4\, \hat{m}^2 \Big[3K_2(\hat{m}) + \hat{m}K_1(\hat{m}) \Big], \qquad P_{(0)}(T) = T n_{(0)}(T)$$

Above conservation laws provide closed system of five equations for five unknown functions: ξ, T, and three independent components of U^μ.

Conservation of total angular momentum:

$$\partial_\mu J^{\mu,\alpha\beta}(x) = 0, \quad J^{\mu,\alpha\beta}(x) = -J^{\mu,\beta\alpha}(x)$$

Total angular momentum consists of orbital and spin parts:

$$J^{\mu,\alpha\beta}(x) = L^{\mu,\alpha\beta}(x) + S^{\mu,\alpha\beta}(x),$$

$$L^{\mu,\alpha\beta}(x) = x^\alpha T^{\mu\beta}(x) - x^\beta T^{\mu\alpha}(x)$$

Since the energy-momentum tensor is symmetric, the conservation of the angular momentum implies the conservation of its spin part.

$$\partial_\lambda J^{\lambda,\mu\nu}(x) = 0, \quad \partial_\mu T^{\mu\nu}(x) = 0 \quad \Longrightarrow \partial_\lambda S^{\lambda,\mu\nu}(x) = T^{\nu\mu}(x) - T^{\mu\nu}(x)$$

Hence, the spin tensor $S^{\mu,\alpha\beta}(x)$ is separately conserved in GLW formulation.

Conservation of spin angular momentum:

$$\partial_\alpha S^{\alpha,\beta\gamma}_{GLW}(x) = 0$$

GLW spin tensor in the leading order of $\omega_{\mu\nu}$ is:

$$S^{\alpha,\beta\gamma}_{GLW} = \cosh(\xi)\left(n_{(0)}(T)U^\alpha\omega^{\beta\gamma} + S^{\alpha,\beta\gamma}_{\Delta GLW}\right)$$

Here, $\omega^{\beta\gamma}$ is known as spin polarization tensor, whereas the auxiliary tensor $S^{\alpha,\beta\gamma}_{\Delta GLW}$ is:

$$S^{\alpha,\beta\gamma}_{\Delta GLW} = \mathcal{A}_{(0)}\, U^\alpha U^\delta U^{[\beta}\omega^{\gamma]}{}_\delta$$
$$+\mathcal{B}_{(0)}\left(U^{[\beta}\Delta^{\alpha\delta}\omega^{\gamma]}{}_\delta + U^\alpha\Delta^{\delta[\beta}\omega^{\gamma]}{}_\delta + U^\delta\Delta^{\alpha[\beta}\omega^{\gamma]}{}_\delta\right),$$

with,

$$\mathcal{B}_{(0)} = -\tfrac{2}{\hat{m}^2}s_{(0)}(T)$$

$$\mathcal{A}_{(0)} = -3\mathcal{B}_{(0)} + 2n_{(0)}(T)$$

Basis for boost invariant and transversely homogeneous systems:

For our calculations, it is useful to introduce a local basis consisting of following 4-vectors,

$$
\begin{aligned}
U^\alpha &= \frac{1}{\tau}(t,0,0,z) = (\cosh(\eta),0,0,\sinh(\eta))\,, \\
X^\alpha &= (0,1,0,0)\,, \\
Y^\alpha &= (0,0,1,0)\,, \\
Z^\alpha &= \frac{1}{\tau}(z,0,0,t) = (\sinh(\eta),0,0,\cosh(\eta))\,.
\end{aligned}
$$

where, $\tau = \sqrt{t^2 - z^2}$ is the longitudinal proper time and $\eta = \ln((t+z)/(t-z))/2$ is the space-time rapidity.
The basis vectors satisfy the following normalization and orthogonal conditions:

$$
\begin{aligned}
& U \cdot U = 1 \\
X \cdot X &= Y \cdot Y = Z \cdot Z = -1, \\
X \cdot U &= Y \cdot U = Z \cdot U = 0, \\
X \cdot Y &= Y \cdot Z = Z \cdot X = 0.
\end{aligned}
$$

Boost-invariant form for the spin polarization tensor:

We use the following decomposition of the vectors κ^μ and ω^μ,

$$\begin{aligned}\kappa^\alpha &= C_{\kappa U} U^\alpha + C_{\kappa X} X^\alpha + C_{\kappa Y} Y^\alpha + C_{\kappa Z} Z^\alpha,\\ \omega^\alpha &= C_{\omega U} U^\alpha + C_{\omega X} X^\alpha + C_{\omega Y} Y^\alpha + C_{\omega Z} Z^\alpha.\end{aligned}$$

Here the scalar coefficients are functions of the proper time (τ) only due to boost invariance. Since $\kappa \cdot U = 0, \quad \omega \cdot U = 0$, therefore

$$\begin{aligned}\kappa^\alpha &= C_{\kappa X} X^\alpha + C_{\kappa Y} Y^\alpha + C_{\kappa Z} Z^\alpha,\\ \omega^\alpha &= C_{\omega X} X^\alpha + C_{\omega Y} Y^\alpha + C_{\omega Z} Z^\alpha.\end{aligned}$$

$\omega_{\mu\nu} = \kappa_\mu U_\nu - \kappa_\nu U_\mu + \epsilon_{\mu\nu\alpha\beta} U^\alpha \omega^\beta$ can be written as,

$$\begin{aligned}\omega_{\mu\nu} &= C_{\kappa Z}(Z_\mu U_\nu - Z_\nu U_\mu) + C_{\kappa X}(X_\mu U_\nu - X_\nu U_\mu) + C_{\kappa Y}(Y_\mu U_\nu - Y_\nu U_\mu)\\ &\quad + \epsilon_{\mu\nu\alpha\beta} U^\alpha (C_{\omega Z} Z^\beta + C_{\omega X} X^\beta + C_{\omega Y} Y^\beta)\end{aligned}$$

In the plane $z = 0$ we find:

$$\omega_{\mu\nu} = \begin{bmatrix} 0 & C_{\kappa X} & C_{\kappa Y} & C_{\kappa Z} \\ -C_{\kappa X} & 0 & -C_{\omega Z} & C_{\omega Y} \\ -C_{\kappa Y} & C_{\omega Z} & 0 & -C_{\omega X} \\ -C_{\kappa Z} & -C_{\omega Y} & C_{\omega X} & 0 \end{bmatrix}$$

Boost-Invariant form of fluid dynamics with spin:

- Conservation law of charge can be written as:

$$U^\alpha \partial_\alpha n + n \partial_\alpha U^\alpha = 0$$

Therefore, for Bjorken type of flow we can write,

$$\dot{n} + \frac{n}{\tau} = 0$$

- Conservation law of energy-momentum can be written as:

$$U^\alpha \partial_\alpha \varepsilon + (\varepsilon + P) \partial_\alpha U^\alpha = 0$$

Hence for the Bjorken flow,

$$\dot{\varepsilon} + \frac{(\varepsilon + P)}{\tau} = 0$$

Boost-Invariant form of fluid dynamics with spin:

Using the equations,

$$S^{\alpha,\beta\gamma}_{\Delta GLW} = \mathcal{A}_{(0)} U^\alpha U^\delta U^{[\beta}\omega^{\gamma]}{}_\delta$$
$$+\mathcal{B}_{(0)} \left(U^{[\beta}\Delta^{\alpha\delta}\omega^{\gamma]}{}_\delta + U^\alpha \Delta^{\delta[\beta}\omega^{\gamma]}{}_\delta + U^\delta \Delta^{\alpha[\beta}\omega^{\gamma]}{}_\delta \right),$$

and

$$S^{\alpha,\beta\gamma}_{GLW} = \cosh(\xi) \left(n_{(0)}(T) U^\alpha \omega^{\beta\gamma} + S^{\alpha,\beta\gamma}_{\Delta GLW} \right)$$

in

$$\partial_\alpha S^{\alpha,\beta\gamma}_{GLW}(x) = 0$$

Contracting the final equation with $U_\beta X_\gamma, U_\beta Y_\gamma, U_\beta Z_\gamma, Y_\beta Z_\gamma, X_\beta Z_\gamma$ and $X_\beta Y_\gamma$.

$$\begin{bmatrix} \mathcal{L}(\tau) & 0 & 0 & 0 & 0 & 0 \\ 0 & \mathcal{L}(\tau) & 0 & 0 & 0 & 0 \\ 0 & 0 & \mathcal{L}(\tau) & 0 & 0 & 0 \\ 0 & 0 & 0 & \mathcal{P}(\tau) & 0 & 0 \\ 0 & 0 & 0 & 0 & \mathcal{P}(\tau) & 0 \\ 0 & 0 & 0 & 0 & 0 & \mathcal{P}(\tau) \end{bmatrix} \begin{bmatrix} \dot{C}_{\kappa X} \\ \dot{C}_{\kappa Y} \\ \dot{C}_{\kappa Z} \\ \dot{C}_{\omega X} \\ \dot{C}_{\omega Y} \\ \dot{C}_{\omega Z} \end{bmatrix} = \begin{bmatrix} \mathcal{Q}_1(\tau) & 0 & 0 & 0 & 0 & 0 \\ 0 & \mathcal{Q}_1(\tau) & 0 & 0 & 0 & 0 \\ 0 & 0 & \mathcal{Q}_2(\tau) & 0 & 0 & 0 \\ 0 & 0 & 0 & \mathcal{R}_1(\tau) & 0 & 0 \\ 0 & 0 & 0 & 0 & \mathcal{R}_1(\tau) & 0 \\ 0 & 0 & 0 & 0 & 0 & \mathcal{R}_2(\tau) \end{bmatrix} \begin{bmatrix} C_{\kappa X} \\ C_{\kappa Y} \\ C_{\kappa Z} \\ C_{\omega X} \\ C_{\omega Y} \\ C_{\omega Z} \end{bmatrix},$$

where,

$\mathcal{L}(\tau) = \mathcal{A}_1 - \frac{1}{2}\mathcal{A}_2 - \mathcal{A}_3,$

$\mathcal{P}(\tau) = \mathcal{A}_1,$

$\mathcal{Q}_1(\tau) = -\left[\dot{\mathcal{L}} + \frac{1}{\tau}\left(\mathcal{L} + \frac{1}{2}\mathcal{A}_3\right)\right],$

$\mathcal{Q}_2(\tau) = -\left(\dot{\mathcal{L}} + \frac{\mathcal{L}}{\tau}\right),$

$\mathcal{R}_1(\tau) = -\left[\dot{\mathcal{P}} + \frac{1}{\tau}\left(\mathcal{P} - \frac{1}{2}\mathcal{A}_3\right)\right],$

$\mathcal{R}_2(\tau) = -\left(\dot{\mathcal{P}} + \frac{\mathcal{P}}{\tau}\right).$

$$\mathcal{A}_1 = \cosh(\xi)\left(n_{(0)} - \mathcal{B}_{(0)}\right),$$
$$\mathcal{A}_2 = \cosh(\xi)\left(\mathcal{A}_{(0)} - 3\mathcal{B}_{(0)}\right),$$
$$\mathcal{A}_3 = \cosh(\xi)\,\mathcal{B}_{(0)}$$

Background evolution:

Initial baryon chemical potential $\mu_0 = 800$ MeV
Initial temperature $T_0 = 155$ MeV
Particle (Lambda hyperon) mass $m = 1116$ MeV

Initial and final proper time is $\tau_0 = 1$ fm and $\tau_f = 10$ fm, respectively.

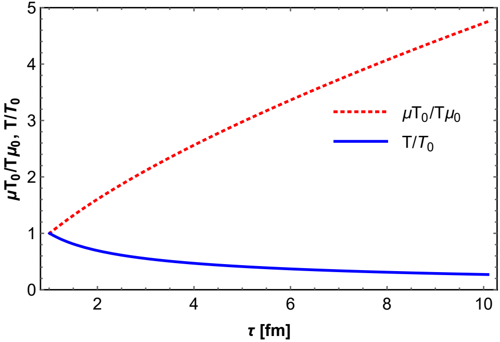

Figure: Proper-time dependence of T divided by its initial value T_0 (solid line) and the ratio of baryon chemical potential μ and temperature T re-scaled by the initial ratio μ_0/T_0 (dotted line) for a boost-invariant one-dimensional expansion.

Spin polarization evolution:

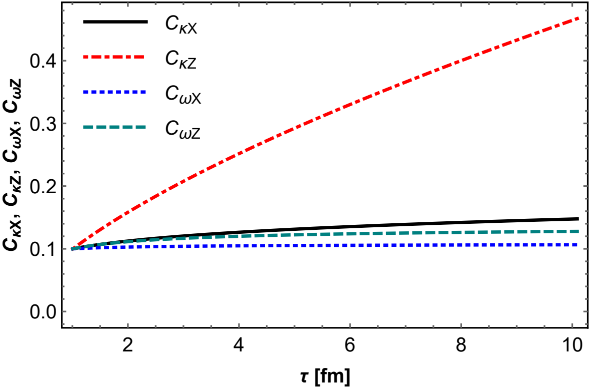

Figure: Proper-time dependence of the coefficients $C_{\kappa X}$, $C_{\kappa Z}$, $C_{\omega X}$ and $C_{\omega Z}$. The coefficients $C_{\kappa Y}$ and $C_{\omega Y}$ satisfy the same differential equations as the coefficients $C_{\kappa X}$ and $C_{\omega X}$.

Spin polarization of particles at the freeze-out:

Average spin polarization per particle $\langle \pi_\mu(p) \rangle$ is given as:

$$\langle \pi_\mu \rangle = \frac{E_p \frac{d\Pi_\mu(p)}{d^3p}}{E_p \frac{d\mathcal{N}(p)}{d^3p}}$$

where, the total value of the Pauli-Lubański vector for particles with momentum p is:

$$E_p \frac{d\Pi_\mu(p)}{d^3p} = -\frac{\cosh(\xi)}{(2\pi)^3 m} \int \Delta\Sigma_\lambda p^\lambda \, e^{-\beta\cdot p} \, \tilde{\omega}_{\mu\beta} p^\beta$$

momentum density of all particles is given by:

$$E_p \frac{d\mathcal{N}(p)}{d^3p} = \frac{4\cosh(\xi)}{(2\pi)^3} \int \Delta\Sigma_\lambda p^\lambda \, e^{-\beta\cdot p}$$

and freeze-out hypersurface is defined as:

$$\Delta\Sigma_\lambda = U_\lambda dxdy \, \tau d\eta$$

Assuming that freeze-out takes place at a constant value of τ and parameterizing the particle four-momentum p^λ in terms of the transverse mass m_T and rapidity y_p, we get:

$$\Delta\Sigma_\lambda p^\lambda = m_T \cosh\left(y_p - \eta\right) dxdy \, \tau d\eta$$

Boost to the local rest frame (LRF) of the particle:

Polarization vector $\langle \pi^{\star}_{\mu} \rangle$ in the local rest frame of the particle can be obtained by using the canonical boost. Using the parametrizations $E_p = m_T \cosh(y_p)$ and $p_z = m_T \sinh(y_p)$ and applying the appropriate Lorentz transformation we get,

$$\langle \pi^{\star}_{\mu} \rangle = -\frac{1}{8m} \begin{bmatrix} 0 \\ \left(\frac{\sinh(y_p) p_x}{m_T \cosh(y_p)+m}\right) \left[\chi \left(C_{\kappa X} p_y - C_{\kappa Y} p_x\right) + 2 C_{\omega Z} m_T\right] + \frac{\chi\, p_x \cosh(y_p)(C_{\omega X} p_x + C_{\omega Y} p_y)}{m_T \cosh(y_p)+m} + 2 C_{\kappa Z} p_y - \chi C_{\omega X} m_T \\ \left(\frac{\sinh(y_p) p_y}{m_T \cosh(y_p)+m}\right) \left[\chi \left(C_{\kappa X} p_y - C_{\kappa Y} p_x\right) + 2 C_{\omega Z} m_T\right] + \frac{\chi\, p_y \cosh(y_p)(C_{\omega X} p_x + C_{\omega Y} p_y)}{m_T \cosh(y_p)+m} - 2 C_{\kappa Z} p_x - \chi C_{\omega Y} m_T \\ -\left(\frac{m \cosh(y_p)+m_T}{m_T \cosh(y_p)+m}\right) \left[\chi \left(C_{\kappa X} p_y - C_{\kappa Y} p_x\right) + 2 C_{\omega Z} m_T\right] - \frac{\chi\, m \sinh(y_p)(C_{\omega X} p_x + C_{\omega Y} p_y)}{m_T \cosh(y_p)+m} \end{bmatrix}$$

where,

$\chi\left(\hat{m}_T\right) = \left(K_0\left(\hat{m}_T\right) + K_2\left(\hat{m}_T\right)\right) / K_1\left(\hat{m}_T\right)$,

$\hat{m}_T = m_T / T$

Momentum dependence of polarization:

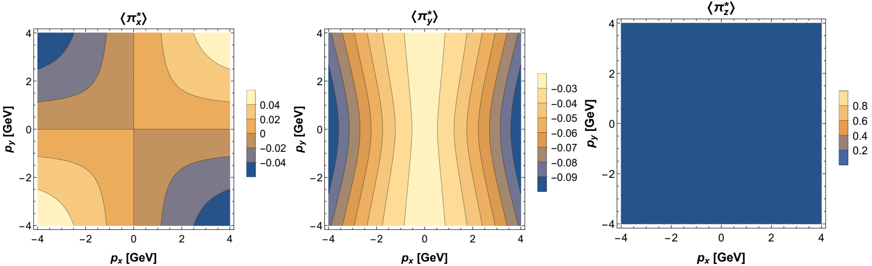

Figure: Components of the PRF mean polarization three-vector of Λ's. The results obtained with the initial conditions $\mu_0 = 800$ MeV, $T_0 = 155$ MeV, $\boldsymbol{C}_{\kappa,0} = (0,0,0)$, and $\boldsymbol{C}_{\omega,0} = (0,0.1,0)$ for $y_p = 0$.

Summary:

- We have discussed relativistic hydrodynamics with spin based on the GLW formulation of energy-momentum and spin tensors.
- For boost invariant and transversely homogeneous set-up we show how our hydrodynamic framework with spin can be used to determine the spin polarization observables measured in heavy ion collisions.
- Since we worked with 0+1 dimensional expansion, our results cannot be compared with the experimental data.
- Our future work is to extend our hydrodynamic approach for 1+3 dimensions and interpret the experimental data correctly.

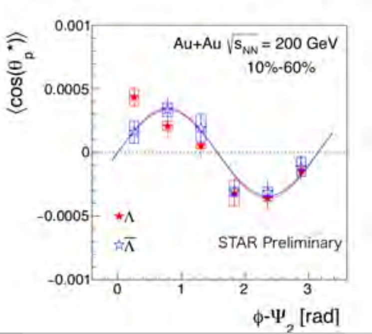

Grazie per l'attenzione!

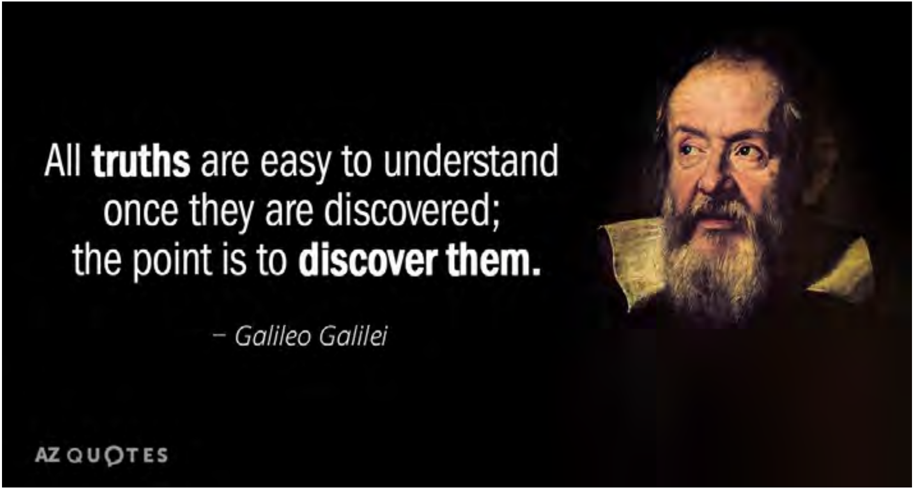

Thank you for your attention!

Back-Up Slides

Measuring polarization in experiment:

Parity-violating decay of hyperons

Daughter baryon is preferentially emitted in the direction of hyperon's spin (opposite for anti-particle)

$$\frac{dN}{d\Omega^*} = \frac{1}{4\pi}(1 + \alpha_H \mathbf{P}_H \cdot \mathbf{p}_p^*)$$

P_H: Λ polarization
p_p^*: proton momentum in the Λ rest frame
α_H: Λ decay parameter
($\alpha_\Lambda = -\alpha_{\bar{\Lambda}} = 0.642 \pm 0.013$)

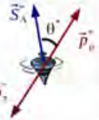

$$\Lambda \to p + \pi^-$$

(BR: 63.9%, cτ~7.9 cm)

C. Patrignani et al. (PDG), Chin. Phys. C 40, 100001 (2016)

Projection onto the transverse plane

Angular momentum direction can be determined by spectator deflection (spectators deflect outwards)
- S. Voloshin and TN, PRC94.021901(R)(2016)

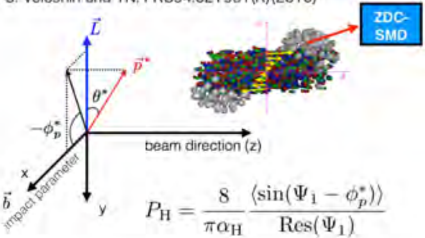

$$P_H = \frac{8}{\pi \alpha_H} \frac{\langle \sin(\Psi_1 - \phi_p^*) \rangle}{\mathrm{Res}(\Psi_1)}$$

Ψ_1: azimuthal angle of b
ϕ_p^*: ϕ of daughter proton in Λ rest frame
STAR, PRC76, 024915 (2007)

Source: T. Niida, WWND 2019

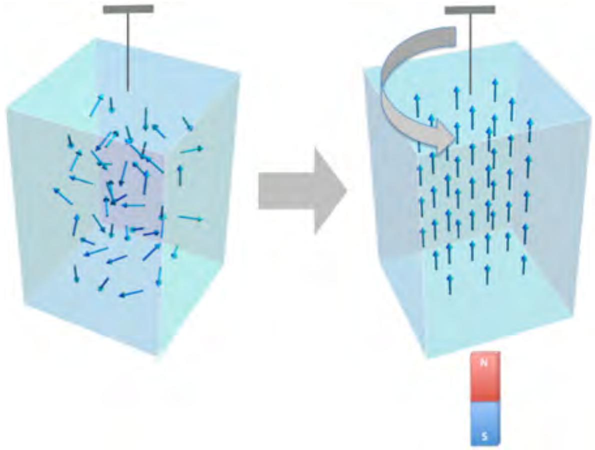

Figure: Einstein-De Haas Effect

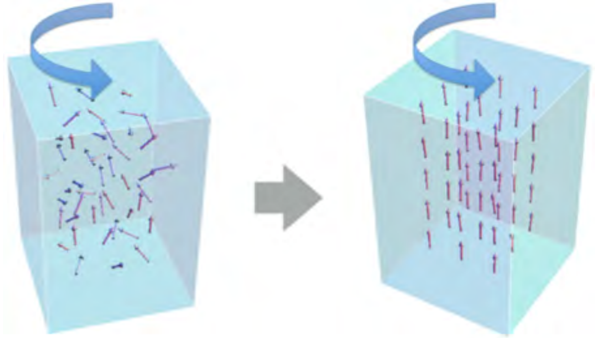

Figure: Barnett Effect

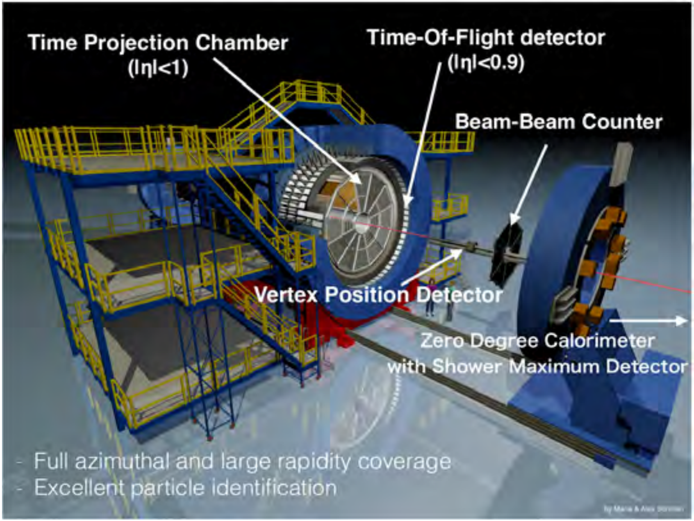

Figure: Schematic view of STAR Detector

Wounded quarks, diquarks and nucleons in heavy-ion collisions

Michał Barej

AGH University of Science and Technology, Kraków, Poland

In collaboration with Adam Bzdak and Paweł Gutowski

Frontiers in Nuclear and Hadronic Physics, Florence 24.02.-06.03.2020

Outline

1. Wounded constituent models
2. Wounded constituent emission function
3. Predictions for $dN_{ch}/d\eta$ compared with PHENIX and PHOBOS data
4. Summary

Particle production in relativistic heavy-ion collisions

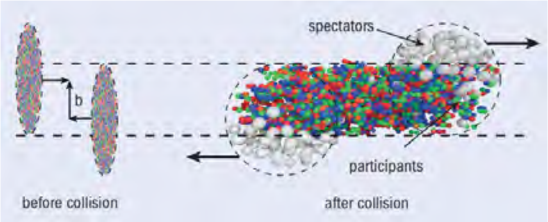

http://cerncourier.com/cws/article/cern/53089

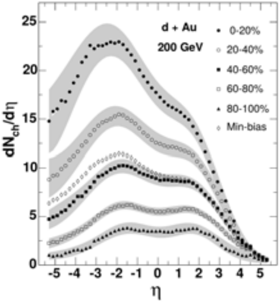

B. Back *et al.* [PHOBOS], Phys. Rev. C 72, 031901 (2005)

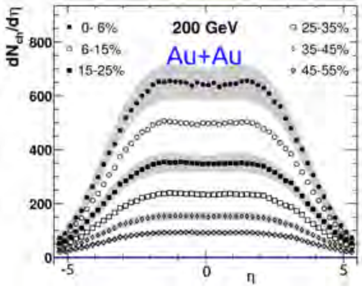

B. Back *et al.* [PHOBOS], Phys. Rev. Lett. 91, 052303 (2003)

Try to describe by wounded nucleon model

- Wounded nucleon model

  A. Bialas, M. Bleszynski and W. Czyz, Nucl. Phys. B **111**, 461 (1976).
- Simple assumptions:
  - Nuclei collision - as a superposition of multiple nucleon-nucleon interactions.
  - For each nucleon from one nucleus check whether it interacts with each nucleon from another nucleus.
  - Each nucleon which interacts with at least one other - wounded.
  - Each wounded nucleon produces particles independently of how many times it was "wounded".
  - $N_{ch} \sim N_{\text{part}}$

Wounded quark model

- A. Bialas, W. Czyz and W. Furmanski, Acta Phys. Polon. B **8**, 585 (1977).
- analogous
- valence quarks (nucleon consists of 3)
- multiple quark-quark interactions
- $N_{ch} \sim$ #wounded quarks

Wounded quark-diquark model

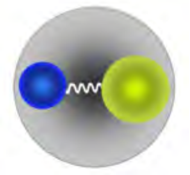

- A. Bialas and A. Bzdak, Phys. Lett. B **649**, 263 (2007)
- analogous
- nucleon consists of a quark and a diquark
- multiple quark-quark, quark-diquark, diquark-diquark interactions
- $N_{ch} \sim$ #wounded quarks and diquarks

- WQDM not only works for particle production but also successfully describes the differential elastic pp cross-section $\frac{d\sigma}{dt}$

  A. Bialas and A. Bzdak, Acta Phys. Polon. B **38**, 159 (2007)

  and extended model, e.g.

  F. Nemes, T. Csörgő and M. Csanád, Int. J. Mod. Phys. A **30**, no. 14, 1550076 (2015)

Common idea for WNM, WQM and WQDM models

- Each wounded constituent emits the number of particles according to the same probability distribution *independently of number of collisions*

$$N(\eta) := \frac{dN_{ch}}{d\eta}(\eta) = w_L F(\eta) + w_R F(-\eta)$$

A. Bialas and W. Czyz, Acta Phys. Polon. B **36**, 905 (2005)

$F(\eta)$ - **wounded constituent emission function**
w_L - mean number of wounded constituents in left-going nucleus
w_R - same for right-going one

- Then (if $w_L \neq w_R$):

$$F(\eta) = \frac{1}{2}\left[\frac{N(\eta) + N(-\eta)}{w_L + w_R} + \frac{N(\eta) - N(-\eta)}{w_L - w_R}\right].$$

- Input: known $dN_{ch}/d\eta$ distribution.
- Numbers of wounded constituents computed in MC simulation.

First step

- $F(\eta) = \frac{1}{2}\left[\frac{N(\eta)+N(-\eta)}{w_L+w_R} + \frac{N(\eta)-N(-\eta)}{w_L-w_R}\right]$
- Take distribution $N(\eta) = dN_{ch}/d\eta$ from d+Au @200 GeV @BNL RHIC by PHOBOS.

Simulation algorithm: MC Glauber based.

- For each nucleus-nucleus collision:
  - Draw nucleons positions from density distibutions.
  - [In WQM and WQDM: draw also quarks (and diquarks) positions around the center of nucleon.]
  - Draw impact parameter b.
  - For each pair check whether the collision happened.
  - For each wounded constituent draw the number of emitted particles according to NBD.
- Divide all events into centrality classes based on the number of produced particles.
- Calculate mean numbers of wounded constituents w_L, w_R in centralities.

Emission functions - wounded quarks

in various centrality classes

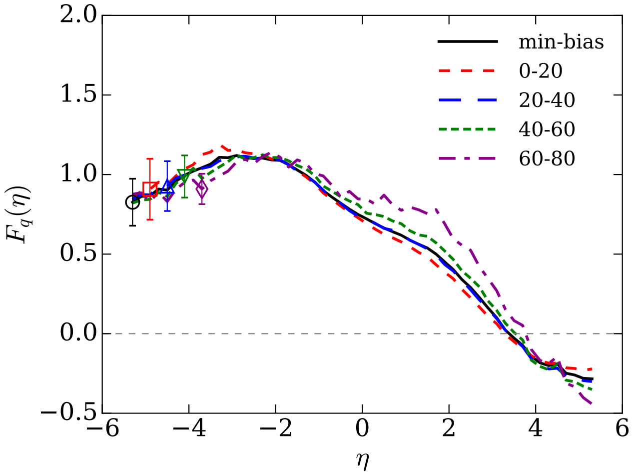

MB, A. Bzdak, P. Gutowski, Phys. Rev. C **97**, no. 3, 034901 (2018)

Min-bias wounded constituent emission functions

- Within uncertainties, the emission functions are same in all centralities.
- $\Rightarrow$ Pick min-bias emission functions $F(\eta)$.

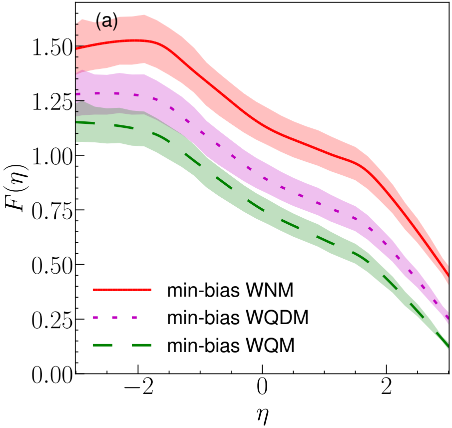

MB, A. Bzdak, P. Gutowski, Phys. Rev. C **100**, no. 6, 064902 (2019)

Next step

- Take extracted min-bias emission functions $F(\eta)$.
- Compute mean numbers of wounded constituents in MC simulation for various systems.
- Predict $dN_{ch}/d\eta$ distributions (assume $F(\eta)$ universal among systems).

$$N(\eta) := \frac{dN_{ch}}{d\eta}(\eta) = w_L F(\eta) + w_R F(-\eta)$$

- Compare with experimental data.

PHENIX measurements on asymmetric collisions

- We were asked by the PHENIX collaboration to make predictions on $dN_{ch}/d\eta$ for asymmetric collisions.
- PHENIX have done dedicated experiments and successfully verified WQM.
- A. Adare *et al.* [PHENIX Collaboration], Phys. Rev. Lett. **121**, no. 22, 222301 (2018)

Asymmetric collisions

p+Au (small + big)

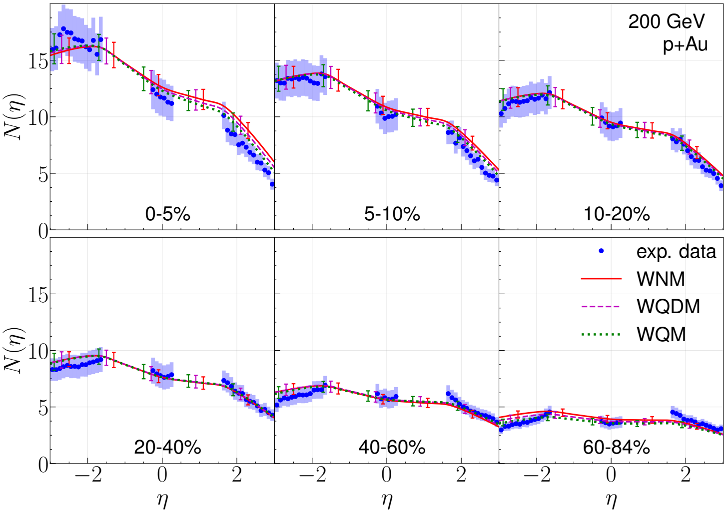

MB, A. Bzdak, P. Gutowski, Phys. Rev. C **100**, no. 6, 064902 (2019)

Data points: A. Adare *et al.* [PHENIX Collaboration], Phys. Rev. Lett. **121**, no. 22, 222301 (2018)

d+Au (small + big)

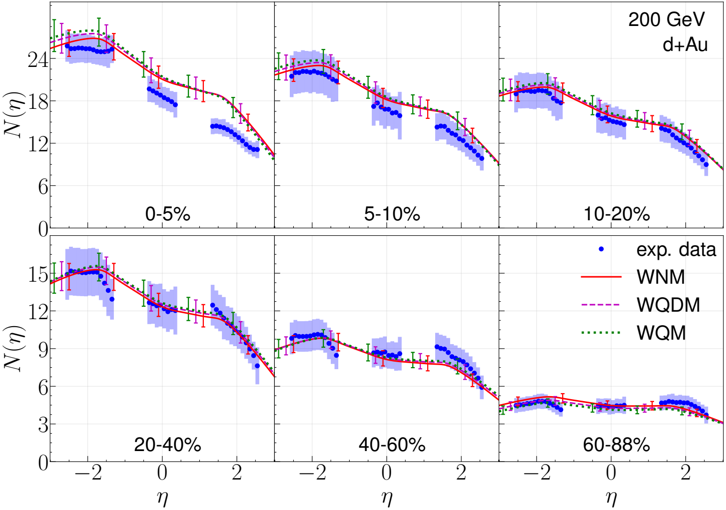

^{3}He+Au (small + big)

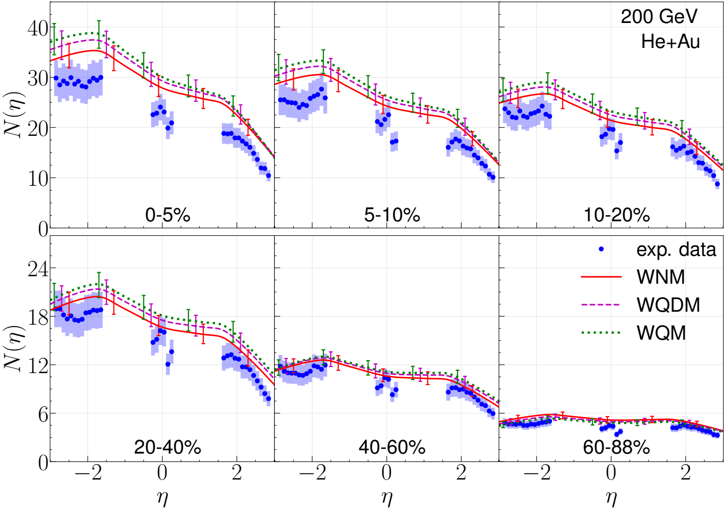

p+Al (small + middle)

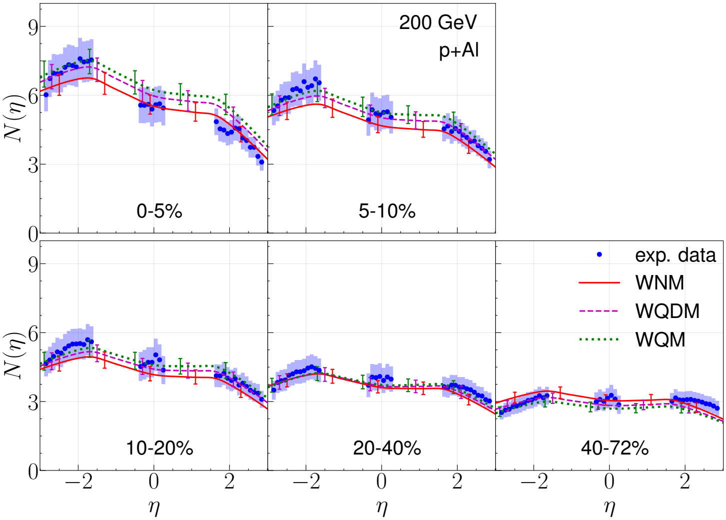

Cu+Au (big + bigger)

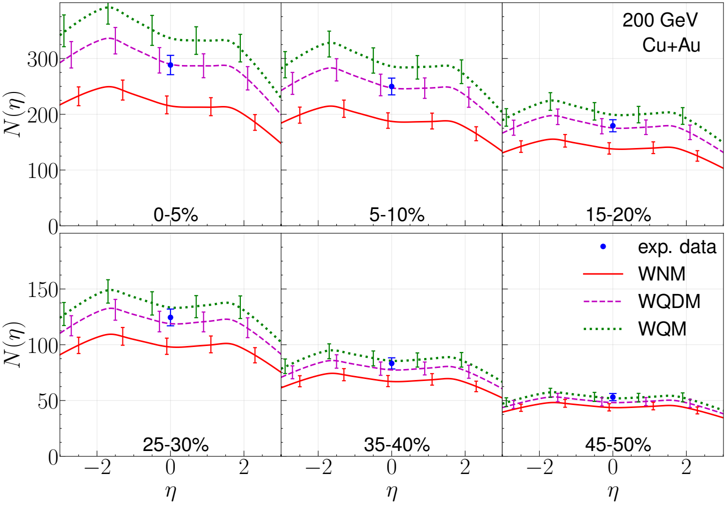

Data points: A. Adare *et al.* [PHENIX Collaboration], Phys. Rev. C **93**, no. 2, 024901 (2016)

Symmetric collisions

Cu+Cu (big + big)

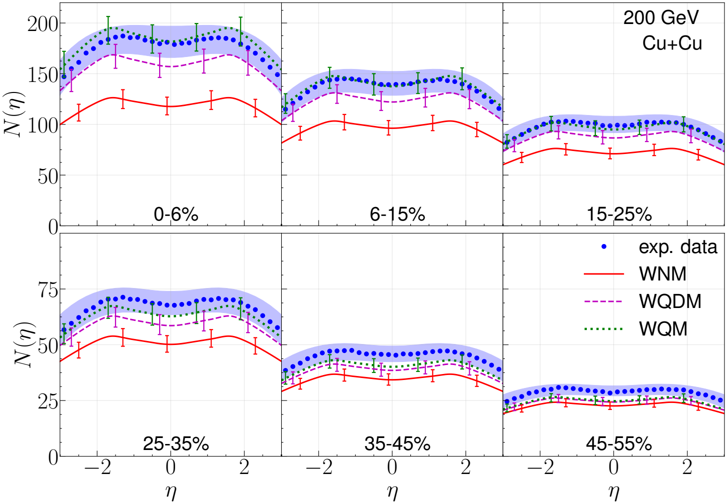

Data points: B. Alver *et al.* [PHOBOS Collaboration], Phys. Rev. Lett. **102**, 142301 (2009)

Au+Au (big + big)

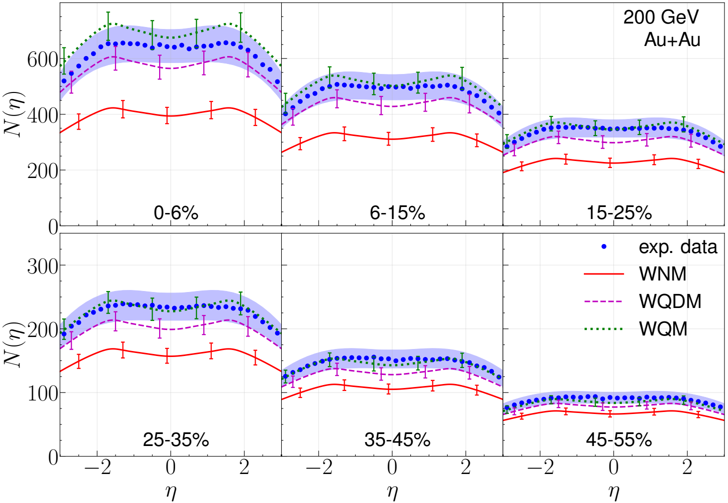

Data points: B. B. Back *et al.*, Phys. Rev. Lett. **91**, 052303 (2003)

U+U (big + big)

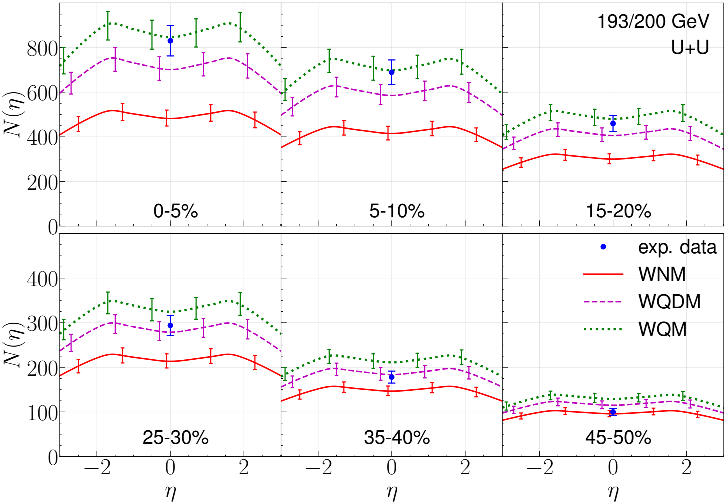

Data points: A. Adare *et al.* [PHENIX Collaboration], Phys. Rev. C **93**, no. 2, 024901 (2016)

p+p (small + small)

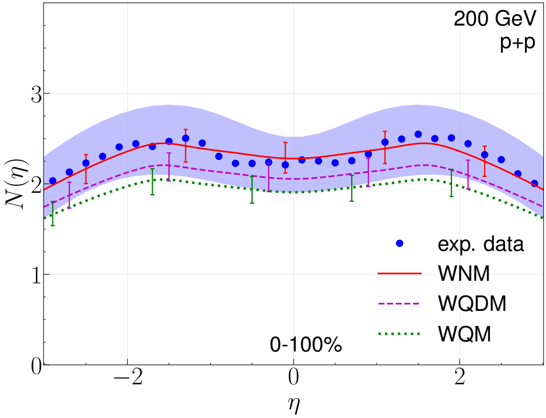

Data points: B. Alver *et al.* [PHOBOS Collaboration], Phys. Rev. C **83**, 024913 (2011)

Summary

- Using $dN_{ch}/d\eta$ data from d+Au @200 GeV by PHOBOS and our MC Glauber simulation, the universal $F(\eta)$ wounded-constituent emission functions were extracted in 3 models.
- WQM and WQDM with $F(\eta)$ work well for all systems predicting $dN_{ch}/d\eta$ consistent with data.
- A minimalistic and almost parameter-free model describes all collisions.
- Possible extensions:
  - Different energies
  - Wider η range (by taking unwounded quarks into account)

Backup

First step

- $F(\eta) = \frac{1}{2}\left[\frac{N(\eta)+N(-\eta)}{w_L+w_R} + \frac{N(\eta)-N(-\eta)}{w_L-w_R}\right]$
- Take distribution $N(\eta) = dN_{ch}/d\eta$ from d+Au @200 GeV @BNL RHIC by PHOBOS.

Simulation algorithm: MC Glauber based.

- For each nucleus-nucleus collision:
  - Draw nucleons positions from density distibutions.
  - [In WQM and WQDM: draw also quarks (and diquarks) positions around the center of nucleon.]
  - Draw impact parameter b.
  - For each pair check whether the collision happened.
  - For each wounded constituent draw the number of emitted particles according to NBD.
- Divide all events into centrality classes based on the number of produced particles.
- Calculate mean numbers of wounded constituents w_L, w_R in centralities.

Simulation details

- Nucleons positions
  - Au, Cu: Woods-Saxon
  - d: Hulthen
  - Deformed nuclei Al, U: generalized W-Sax (no spherical symmetry)
- Quarks positions: $\varrho(\vec{r}) = \varrho_0 \exp\left(-\frac{r}{a}\right)$

  S. S. Adler *et al.* [PHENIX Collaboration], Phys. Rev. C **89**, no. 4, 044905 (2014)
- Impact parameter: b^2 from uniform on $[0, b^2_{max}]$
- Check whether it was a collision: $u < \exp\left(-\frac{s^2}{2\gamma^2}\right), \quad \gamma^2 = \sigma/(2\pi)$

  σ - cross section:
  - $\sigma_{nn} = 41$ mb in WNM
  - $\sigma_{qq} = 6.65$ mb in WQM
  - $\sigma_{qq} = 5.75$ mb in WQDM with $\sigma_{\mathrm{qq}} : \sigma_{\mathrm{qd}} : \sigma_{\mathrm{dd}} = 1 : 2 : 4$

Simulation details

- Charged particle production
  - Each wounded nucleon populates number of particles according to NBD with $\langle n \rangle = 5$ oraz $k = 1$
  - In case of WQM and WQDM divide $\langle n \rangle$ and k by 1.27 and 1.14, respectively (mean number of wounded constituents per a wounded nucleon).

Emission functions - wounded nucleons

in various centrality classes

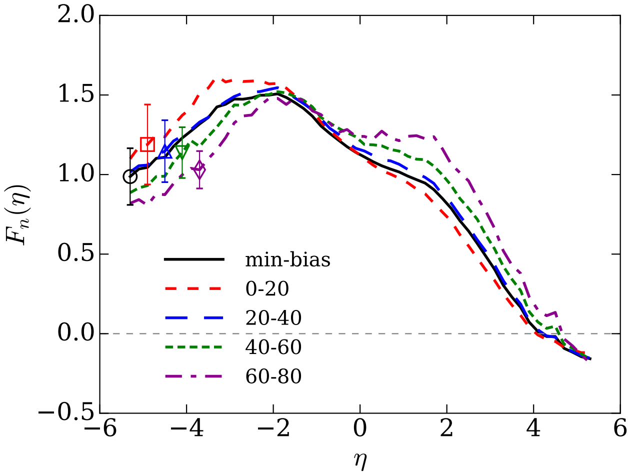

MB, A. Bzdak, P. Gutowski, Phys. Rev. C **97**, no. 3, 034901 (2018)

WNM is invalid

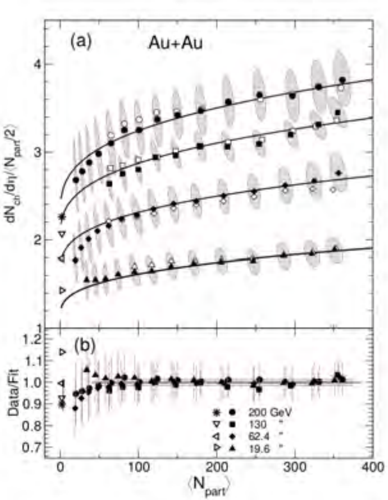

B. Alver *et al.* [PHOBOS Collaboration], Phys. Rev. C **83**, 024913 (2011)

- WNM:

$$\frac{N_{ch}}{N_{part}} = \text{const}$$

- Data: $\frac{N_{ch}}{N_{part}} \sim \left(1 + cN_{part}^{1/3}\right)$
- Try to introduce:

$$\frac{N_{ch}}{N_{part}} \neq \text{const}$$

  by N_{coll} dependence.
- WQ(D)M and WNM + N_{coll} both have the same goal but different physics under it.
- Models differ at large N_{coll}

Explain $N_{part}^{1/3}$ dependence qualitatively

- $V_A \sim N_{part} V_n \sim R^3$
- $R \sim N_{part}^{1/3}$
- $N_{coll} \sim N_{part} \cdot N_{part}^{1/3} = N_{part}^{4/3}$
- $N_{ch} \sim N_{coll}$
- $\frac{N_{ch}}{N_{part}} \sim N_{part}^{1/3}$

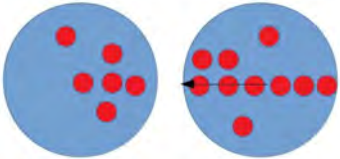

v_2 vs normalized multiplicity

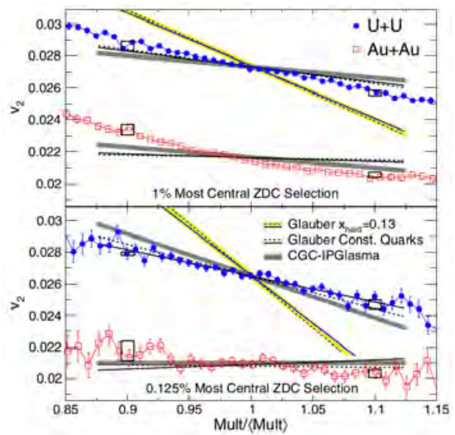

L. Adamczyk *et al.* [STAR Collaboration], Phys. Rev. Lett. **115**, no. 22, 222301 (2015)

- Used control sample of Au+Au collisions (v_2 should be const at given centrality).
- Normalized multiplicity (different size of Au and U).
- 0-1% centrality: still dependence on centrality (see Au)
- 0-0.125% centrality: dependence mostly on geometry.
  Here multiplicity varies due to tip-tip or body-body etc.

v_2 vs normalized multiplicity

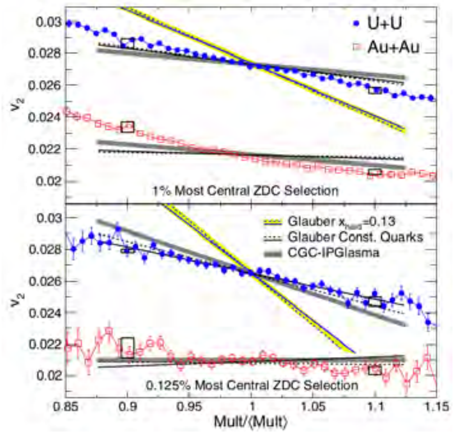

L. Adamczyk *et al.* [STAR Collaboration], Phys. Rev. Lett. **115**, no. 22, 222301 (2015)

- WNM + N_{coll}:

  $N_{ch} \sim (1 - x_{hard})\frac{N_{part}}{2} + x_{hard} N_{coll}$

  D. Kharzeev and M. Nardi, Phys. Lett. B **507**, 121 (2001)

  overpredicts the slope assuming big contribution of N_{coll}
- WQM gives good results! (CGC IP-Glasma does too)
- indirect N_{coll} dependence, smaller contribution.

Unwounded quarks in wounded nucleons

- Nucleon is wounded if at least one of its quarks is wounded
- If e.g. 1 quark is wounded, there are 2 more unwounded quarks remaining!

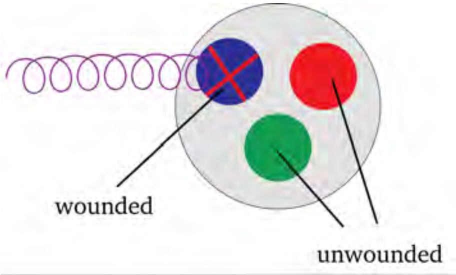

- A. Białas, A. Bzdak, Phys. Lett. B **649**, 263 (2007)

Unwounded quarks in wounded nucleons

- Add terms in multiplicity equation:

$$N(\eta) = w_L F(\eta) + w_R F(-\eta) + \boldsymbol{\overline{w}_L U(\eta) + \overline{w}_R U(-\eta)}$$

$\overline{w}_L$, $\overline{w}_R$ - mean numbers of unwounded quarks from wounded nucleons in left- and right-going nucleus, respectively

$U(\eta)$ - emission function of an unwounded quark from wounded nucleon

- WQM: $w_q + \overline{w}_q = 3w_n$
- $U(\eta)$ not significant as long as $|\eta| < 3$.
- $U(\eta)$ can be extracted:

$$U(\eta) = \frac{\overline{w}_L N(\eta) - \overline{w}_R N(-\eta) - (w_L \overline{w}_L - w_R \overline{w}_R) F(\eta) + (w_R \overline{w}_L - w_L \overline{w}_R) F(-\eta)}{(\overline{w}_L + \overline{w}_R)(\overline{w}_L - \overline{w}_R)}$$

Unwounded quarks in wounded nucleons

$$N(\eta) = w_L F(\eta) + w_R F(-\eta) + \boldsymbol{\overline{w}_L U(\eta) + \overline{w}_R U(-\eta)}$$

$$U(\eta) = \frac{\overline{w}_L N(\eta) - \overline{w}_R N(-\eta) - (w_L \overline{w}_L - w_R \overline{w}_R) F(\eta) + (w_R \overline{w}_L - w_L \overline{w}_R) F(-\eta)}{(\overline{w}_L + \overline{w}_R)(\overline{w}_L - \overline{w}_R)}$$

- In order to extract $U(\eta)$ you need:
  - $\overline{w}_L \neq \overline{w}_R$ - asymmetric collision
  - $dN_{ch}/d\eta$ in wide η range
  - to postulate $F(\eta)$ for $|\eta| > 3$, e.g.:

$$\widetilde{F}(\eta) = \begin{cases} 0, & \eta < -\eta_0 - \Delta\eta \\ a\eta + b, & -\eta_0 - \Delta\eta \leq \eta < -\eta_0 \\ F(\eta), & |\eta| \leq \eta_0 \\ 0, & \eta > \eta_0 \end{cases}$$

  - Compare with data and look for good $F(\eta)$ for $|\eta| > 3$ postulate.

Unwounded quarks in wounded nucleons - only trial

$$N(\eta) = w_L F(\eta) + w_R F(-\eta) + \boldsymbol{\overline{w}_L U(\eta) + \overline{w}_R U(-\eta)}$$

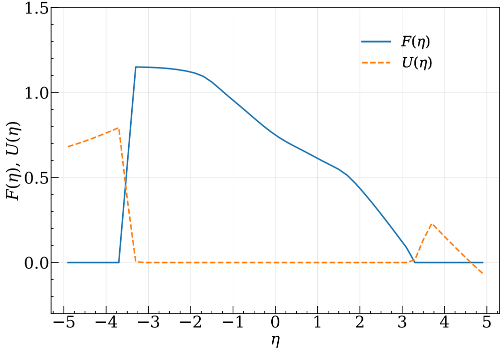

$$\widetilde{F}(\eta) = \begin{cases} 0, & \eta < -\eta_0 - \Delta\eta \\ a\eta + b, & -\eta_0 - \Delta\eta \leq \eta < -\eta_0 \\ F(\eta), & |\eta| \leq \eta_0 \\ 0, & \eta > \eta_0 \end{cases}$$

- $\eta_0 = 3.3$
  $\Delta\eta = 0.4$
- $U(\eta)$ should be 0 for $\eta > 0$
  uncertainties + postulated $F(\eta)$
- Good starting point for further research.

WQDM for the elastic pp $\frac{d\sigma}{dt}$

Original model introduced for 23-62 GeV energies

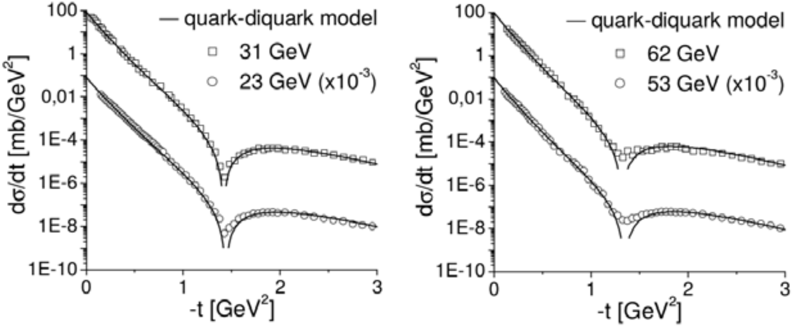

A. Bialas and A. Bzdak, Acta Phys. Polon. B **38**, 159 (2007) [hep-ph/0612038]

WQDM for the elastic pp $\frac{d\sigma}{dt}$

Extended model for TeV energies

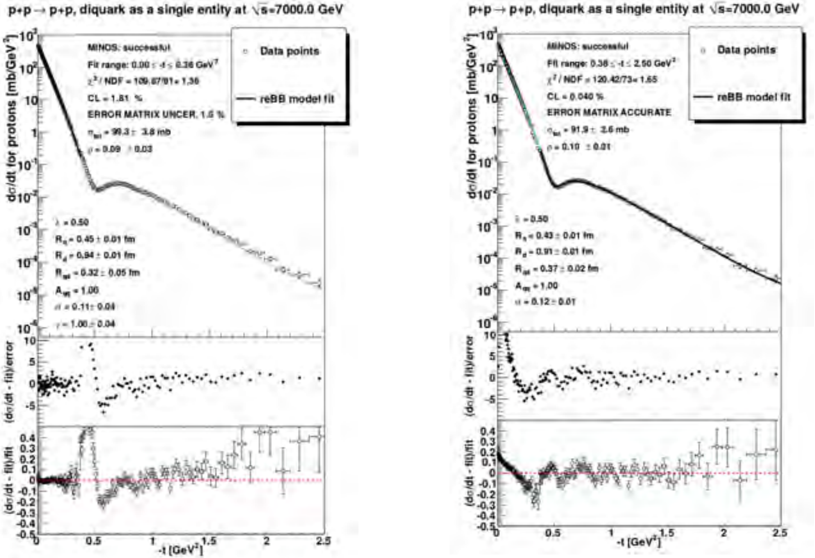

F. Nemes, T. Csörgő and M. Csanád, Int. J. Mod. Phys. A **30**, no. 14, 1550076 (2015)